Akademie věd
České republiky

Thesis of Dissertation for Obtaining the 'Doctor of Sciences' Degree in the Category of the Sciences ***Chemistry***

Structure and Dynamics of Multicomponent Macromolecular and Supramolecular Solids at Atomic Resolution:

From Separation of Local Fields and ^{1}H Spin Diffusion Analysis to Domain-Selective NMR Crystallography

Commission for the Doctoral Dissertation Defense in the Field

Macromolecular Chemistry

Applicant's Name: **Ing. Jiří Brus, Dr.**

Workplace of Applicant: Institute of Macromolecular Chemistry, CAS
Heyrovského nám. 2
162 00 Prague 6
Czech Republic

Place and Date: Prague, 1st August 2023.

Summary of DSc Dissertation:

Structure dictates properties, and "*The ability to accurately predict the structure of complex molecular systems and to relate that structure to properties and reactivity*" remains one of the most important issues in contemporary chemistry. Modern materials science systematically combines a variety of organic, inorganic, polymeric and ceramic materials in an effort to find synergies and develop advanced materials. In this context, multi-component polymer-based nanocomposites and nanostructured solids have attracted considerable attention. However, the true potential of these materials has not yet been fully exploited. In addition to formulating state-of-the-art supramolecular synthesis, further development of these systems requires precise structural characterization. This is a stringent requirement because these systems exist on the borderline between crystalline and amorphous solids, for which high-quality diffraction data are inherently unavailable. Consequently, we are balancing the physical and detection limits of traditionally used experimental techniques.

This thesis traces the twenty-year effort of myself and my collaborators in the development and application of solid-state NMR spectroscopy strategies for the description of the structure and dynamics of amorphous, semi-crystalline and crystalline solids, primarily polymeric composites. We have focused on developing experimental strategies that are fast and reliable enough for both academic and industrial laboratories, applicable to multi-component systems, selective enough to provide structural data for each component separately, and sensitive enough to generate structures at the atomic resolution level. Our aim was to develop computational-experimental approaches to domain-selective NMR spectroscopy of multicomponent solids.

Since 2000, we have focused on the application of advanced techniques of high-performance spectroscopy to elucidate the structure of functional materials down to the atomic resolution level and to describe the intermolecular interactions and dynamics in these systems. In this regard, we have systematically explored various combinations of advanced techniques of NMR spectroscopy, vibrational spectroscopy and X-ray diffraction with DFT calculations and data processing with the aim of formulating robust and reliable strategies of structure analysis. Our early studies began on exploring the experimental techniques based on separation local dipolar fields. In this regard we focused on the two-dimensional (2D) ^{1}H wide-line separation (WISE) experiments and precise analysis of ^{1}H-^{1}H spin diffusion with the aim to calculate size of domains of individual components as well as to probe the structure of sub-nanometre-sized fluctuations at interfacial regions. The developed procedures then were applied to a range of polymeric blends, composite networks and hybrid systems, and the knowledge was further used to probe surface hydroxyls on the silica particles, distribution of POSS crosslinking units in epoxide networks as well as distribution of pharmaceutically active compounds in solid polymeric dispersions. Subsequently we focused on the measurements of heteronuclear dipolar interactions such as ^{1}H-^{13}C dipolar profiles with the aim to describe geometry of local motions of molecular segments. In this period, we also dealt with the domain-selective modifications of these experimental techniques for accurate describing internal dynamics of polymer chain in the semi-crystalline nanocomposites modified by clay minerals. This research was aimed to find relations between the segmental dynamics and macroscopic properties of polymeric systems.

Later, we entered into the world of functional materials, amphidynamic molecular machines with stators and rotors, energy-related materials (polymeric electrolytes) and special construction materials, in which metallacarborane nanorotors play a key role. In this context, we have focused on the analysis of the resonance frequencies of quadrupolar nuclei. By combining the experimental measurements of motion-averaged ^{1}H-^{11}B heteronuclear dipolar interactions, ^{11}B-^{11}B and ^{7}Li-^{7}Li double-quantum (DQ) MAS NMR spectra, systematic analysis of DQ build-up dependencies and quantum chemical calculations we discovered diversity of the self-assembly and dynamics processes of metallacarborane nanorotors in different

polymer matrices, and described a novel type of ion-conducting material for *all-solid-state* electrolytes based on the metal-organic frameworks (MOFs). Using state-of-the-art ss-NMR spectroscopy techniques, we have thoroughly investigated the ionic dynamics in the framework channels, described specific interactions between cations, anions and framework segments, and explained the mechanism of ionic conductivity at the atomic resolution level. Similarly, we have described the local structure and distribution of cross-links in boron-modified phenol-formaldehyde resins designed for soft magnetic composites, and understood the interface-induced growth and transformation of polymer-conjugated proto-crystalline phases in aluminosilicate hybrids.

Polymer-based drug-delivery systems then represent a separate part of this dissertation. For real therapeutic applications, a detailed structural analysis of the drugs that are embedded in the polymer matrix is a strict requirement of all the national and international regulatory authorities. This requirement is particularly urgent for the development of the next generation of polymeric micro- and nanoscaled composites, which are not only promising drug-delivery systems, but also materials with hierarchical architecture executing multiple functions. Precise structural analysis of multiphase polymeric nanocomposites, however, remains a challenge even in the presence of high-quality X-ray diffraction data. The presence of multiple crystalline components results in complicated diffraction patterns, the conversion of which into the refined crystal structures is practically unattainable. In this context, we have explored the combination of various domain-selective (T_1-filtered) 2D solid-state NMR techniques with DFT calculations and spectral data processing to formulate a general experimental-computational strategy for monitoring the atomic-resolution structure of the active compound whose domains are incorporated in the polymeric semi-crystalline matrix. In this strategy, by applying T_1-filtered ss-NMR techniques, the individual components differing in segmental dynamics are consistently selected and the corresponding isotropic chemical shifts are determined and explicitly assigned. In the next step, we applied an automated protocol that allows the processing and statistical analysis of extensively large data sets. This way, the experimentally determined NMR parameters are systematically compared with those DFT-calculated for the representative set of crystal structure predictions. As a result of this search, the crystal structures of micro- and nanosized crystallites dispersed in the polymeric matrix are determined. And thus, as a result of our efforts, one of the possible approaches to the *domain-selective and domain-edited ss-NMR spectroscopy (crystallography)* has been designed.

The last part of the thesis is then devoted to the use of factor analysis of ss-NMR spectra of abundant nuclei to identify minority nanocrystalline phases in multicomponent amorphous solids, thus opening up research towards understanding the structural regularities and diversity of the amorphous phase in molecular solids.

Overall, through the synergistic interplay between measurements, calculations and statistical analysis, we have developed integrated strategies that provide otherwise unavailable structural information for complex multi-component systems in different physical states (liquids, solids, gels). The applied combinations of experimental and theoretical approaches allow the determination of the structural arrangements of molecules in situations that are not amenable to conventional spectroscopic techniques.

Table of Contents

1. Introduction

Solid-state NMR spectroscopy is one of the most technologically and methodologically advanced methods of structural analysis available today. The great advantage of NMR spectroscopy stems from its unique selectivity, which allows the differentiation of chemically distinct structural units. NMR spectroscopy of solutions and liquids has therefore become an indispensable tool for organic chemists in the characterization of newly synthesized molecules. In the solid state, however, the lack of isotropic molecular motion due to a variety of anisotropic interactions, such as chemical shift anisotropy, dipolar and quadrupolar interactions, leads to a dramatic broadening of the signals, and a significant reduction in resolution. In addition, the high strength of these interactions made many techniques commonly used in liquid state NMR (e.g. multidimensional correlation experiments) virtually inapplicable to the study of solids. Although the resulting spectrum is almost impossible for us to read, it is by no means devoid of content. The anisotropic interactions contain valuable structural information, but the spectrum obtained is oversaturated with them. Their influence must therefore be eliminated and separated.

Over the last two decades a number of techniques have been developed to remove the influence of anisotropic interactions at some stage of an NMR experiment, to be in the next step used to accurately determine inter-nuclear distances, torsion angles or to assess molecular dynamics. Technical improvements in ss-NMR probes, allowing magic angle spinning (MAS) of the sample up to frequencies of ca. 110 kHz, have also greatly facilitated the achievement of high resolution ^{1}H NMR spectra. This, combined with the recently developed and optimized homonuclear decoupling pulse sequences, has allowed the design of many advanced multidimensional correlation and separation experiments. Semi-quantitative and quantitative information on specific interatomic distances (e.g. ^{1}H-^{1}H) is provided by very promising double-quantum (DQ) MAS NMR experiments, which allow hydrogen or pi-pi interactions to be distinguished. However, the techniques of solid-state NMR spectroscopy do not only allow the determination of inter-nuclear distances in the range of tens to units of Angstroms. Special long-range experiments have also been developed to quantitatively describe the sizes of individual components in heterogeneous or nano-heterogeneous systems in the range of 1 to 100 nm. It is precisely these techniques and their applications that are the subject of the first parts of this thesis. The techniques discussed do not require isotopic enrichment and are mainly based on dipolar interactions with ^{1}H nuclei. However, the experimental approaches that make it possible to study the local geometry and the interatomic distance of quadrupolar nuclei are also introduced, and they discussed in detail in next sections.

The present dissertation traces more than twenty years of efforts by myself and my collaborators to develop and apply techniques and strategies of solid-state NMR spectroscopy to describe the structure and dynamics of a range of organic, inorganic and hybrid solids, primarily the partially ordered and semi-crystalline composites and functional materials. We have systematically explored different ss-NMR techniques and computational concepts with the aim of finding optimal experimental strategies that are fast and reliable enough for academic and industrial laboratories, applicable to multi-component systems, sufficiently selective to provide structural data for each component individually, and sensitive to generate structures at atomic resolution.

2. ^{1}H Wide-line NMR spectroscopy and ^{1}H-^{1}H spin diffusion

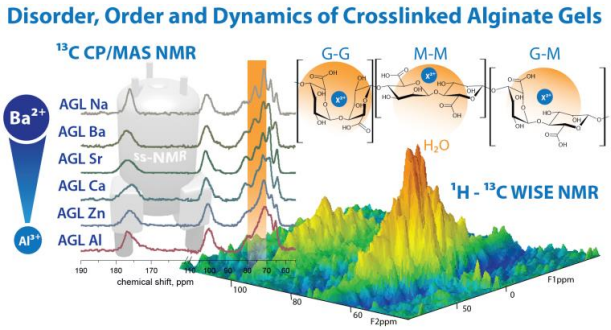

Experimental strategies based on the separation of local dipolar fields represent a type of NMR experiment that allows specific information about the strength of dipolar interactions to be assigned to each resolved molecular segment. In this context, we focused on two-dimensional (2D) ^{1}H wide-line separation experiments (WISE), and precise analysis of ^{1}H-^{1}H spin diffusion to study differences in the segmental dynamics of polymer chains and to calculate the size of the domains they occupy in heterogenous systems. The developed procedures were applied to a number of polymer blends, networks, hybrids and biopolymers, and the knowledge was further used to study the structure of interfacial regions, the arrangement of surface hydroxyls and crosslinking units, and the distribution of drugs in solid polymer dispersions.

2.1. Introduction to the basics - ^{1}H spins in solid-state NMR

The great advantage of NMR spectroscopy is its unique selectivity, which allows to distinguish chemically distinct sites based on their *chemical shielding*. For solution state NMR, protons are the most important nuclei due to their almost 100% natural abundance and the highest gyromagnetic ratio γ. This gives to ^{1}H the highest sensitivity of any naturally occurring nucleus. However, this combination immensely complicates the recording of ^{1}H NMR spectra in the solid state. In the absence of fast molecular tumbling, anisotropic interactions come into play, causing a strong broadening of NMR signals. In solid-state ^{1}H NMR, the dominant anisotropic interactions, which are ^{1}H-^{1}H dipolar couplings, completely prevent the resolution of chemically distinct sites. However, the lack of resolution does not mean the absence of information. The spectra are overcrowded by them that we are unable to read them. For this reason, various techniques have been proposed to increase the spectral resolution of ^{1}H ss-NMR spectra.

Magic Angle Spinning (MAS). One possible way how to compensate missing molecular motion is mechanical rotation. Anisotropic interactions such as dipolar coupling between a pair of nuclei or chemical shift anisotropy (CSA) have an orientation dependence that can be described by the second rank tensor. In such a case physical rotation of the sample around the axis, which is inclined at the angle 54.7° (magic angle) with respect to static magnetic field, leads to the averaging of anisotropy broadening to zero.[1] In that case the originally broad NMR signal is easily broken up into a narrow central signal, reflecting isotropic chemical shift, and a set of spinning-side bands. However, in the case of a strongly coupled multibody ^{1}H spin system, the linewidths of ^{1}H signals remain large even at very fast spinning speeds (Figure 1A). Although the highest spinning frequencies currently achieved are around 110 kHz, the resolution is still not comparable with the resolution obtained for liquids. In addition, the high spinning speeds cause considerable frictional heating (up to 60 K) and the temperature gradients.[2,3] Therefore, alternative methods are continuously developed and applied.

Combined Rotation and Multiple-pulse Spectroscopy (CRAMPS). In this context, the first classical homodecoupling technique (WHH-4) was designed in 1968.[4] It consists of many cycles of solid-echo pulse pairs separated by windows of duration τ or 2τ (Figure 1B). After a cycle of 6τ the spins effectively evolve under the average Hamiltonian reflecting only chemical shift, while the dipolar broadening is suppressed. Stroboscopic detection at these times then produces a narrow signal. Well-resolved ^{1}H MAS NMR spectra (Figure 1A) are then achieved by simultaneous application of MAS refocusing chemical shift anisotropy.[5] Later developed Frequency-Switched and Phase Modulated Lee-Goldburg homodecoupling sequences (FSLG, and PMLG) allowed implementation of various high-resolution ^{1}H-^{1}H and ^{1}H-^{13}C NMR correlation experiments in solid-state.[6] In 2000 a numerically-optimized sequence DUMBO

was developed[7] which, together with stable high-field spectrometers, considerably simplified measurements of high-resolution ^{1}H ss-NMR spectra. However, resolution of ^{1}H ss-NMR spectra is still limited by the intrinsically imperfect nature of coherent averaging. For this reason, new approaches based on the mapping of the error terms are being explored.[8,9]

^{1}H-^{1}H spin-diffusion

On the other hand, the ^{1}H-^{1}H dipolar interactions provide valuable structural information. For example, the spatial transfer of ^{1}H "*z*" magnetization between dipolar-coupled spins, termed "spin exchange" or "spin diffusion", carries information about both the interatomic distances and the size of domains in heterogeneous systems.[10,11] The typical ^{1}H-^{1}H spin-diffusion experiment consists of an evolution or selection period, a mixing period t_m, and a detection period. During the selection period the magnetization of one component is selected, while the magnetization of the second component is suppressed. The mixing period then allows the selected magnetization is transferred to neighboring spins. At short mixing times, ^{1}H polarization is transferred between the nearest spins, while at longer times, relayed polarization transfer to further spins occurs at a rate proportional to $1/r_{ij}^3$ (Figure 1C). Consequently, the detection of spin-exchange process at very short mixing times allows signal assignment and measurement of short-range distances for the molecular structure determination, while the relayed long-range ^{1}H-^{1}H spin exchange (spin diffusion) makes it possible to study objects on 0.5-200 nm scale.[12]

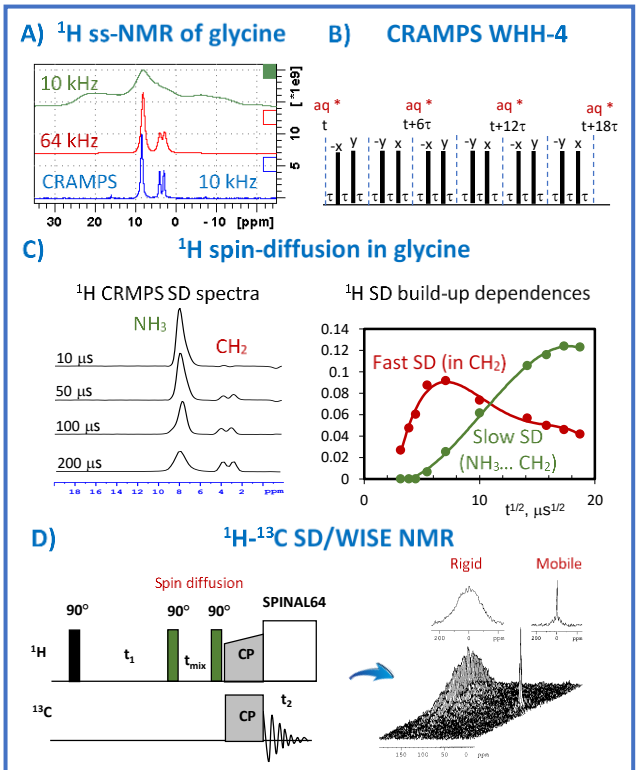

Figure 1. *^{1}H ss-NMR spectra of glycine measured under different conditions (A); WHH-4 pulse sequence (B); ^{1}H-^{1}H spin diffusion in glycine monitored in ^{1}H CRAMPS spectra and the build-up curves (C); ^{1}H-^{13}C SD/WISE pulse sequence and the ^{1}H-^{13}C WISE spectrum illustrating mobile and rigid segments.*

^{1}H wide line separation

As mentioned above, in the absence of segmental motion a broad signal with a line width of several tens of kHz is usually observed in ^{1}H NMR spectra. With increasing segmental dynamics, the ^{1}H linewidth gradually narrows and the ^{1}H signals with a linewidth of about 5-1 kHz indicate partially released motions typical for amorphous polymeric solids above and close to T_g. The ^{1}H MAS spectra with the signals of about 500-50 Hz then reflect soft amorphous elastomers or gels, whereas highly mobile melts, liquids of solutions are characterized by the narrowed signals below 50 Hz. It is thus clear that the ^{1}H linewidth allows direct monitoring of the segmental dynamics, and if the ^{1}H linewidth is accurately separated and correctly correlated with molecular segments, then the proton line shapes can provide a complex picture of the internal dynamics of even complicated multicomponent solids.

This basic idea was followed by Klaus Schmidt-Rohr, who in 1992 developed an easy-to-implement 2D ^{1}H wide-line separation NMR experiment (WISE), which separates ^{1}H dipolar wide-line signals according to ^{13}C chemical shifts (Figure 1D).[13] The first ^{1}H 90° pulse creates ^{1}H magnetization, which evolves during the t_1 period under the influence of ^{1}H-^{1}H dipolar interactions. This causes dephasing of proton magnetization, which results in the loss of ^{1}H signal intensity at the end of the t_1 period. In the next step the residual ^{1}H magnetization is transferred to the ^{13}C spins by the cross-polarization step (CP). The resulting ^{13}C NMR signal is then detected. By incrementing the t_1 period the process of ^{1}H magnetization dephasing is

monitored. In the rigid segments the dephasing is fast and Fourier transformation of this rapid exponential decay results in a broad ^{1}H NMR signal. In contrast, mobile segments lose their ^{1}H coherence slowly and thus the resulting ^{1}H NMR signal is narrow. For illustration the 2D ^{1}H-^{13}C WISE NMR spectrum of a two-component polymer system with rigid aromatic segments and mobile methyl groups is demonstrated in Figure 1D (right). The experiment can be further extended by incorporating the mixing period t_m between the evolution period t_1 and CP block. This way, the ^{1}H-^{1}H spin diffusion becomes active and ^{1}H magnetization is transferred between different segments. As a result, the narrow ^{1}H signal appears on the originally broad ^{1}H line and *vice versa*. And thus, when the ^{1}H WISE NMR spectra are measured with prolonging mixing times t_m (ca. 0.1-50 ms), the intensity of the narrow signal gradually increases and the spin diffusion build-up curves can be constructed. By analyzing this dependence, the size of domains in multi-component systems can be determined.[12-14]

In summary, the experimental approaches outlined above provided a highly efficient instrument that we have used over the past two decades to investigate the internal architecture and morphology of a truly broad range of materials including organic and inorganic solids as well as hybrid polymeric composites.

2.2. Order and mobility in polymeric blends and networks (D1-D4)

Typically, we applied the above-introduced experimental approach to investigate global architecture of polymer blends such as polycarbonate and polyethylenoxide (PC-PEO) [D1]. While the broad ^{1}H signals with the line-width of ca. 30 kHz reflected rigid character of PC segments, the narrow ^{1}H NMR signal separated for PEO units indicated their high mobility (Figure 2A). Huge differences in the ^{1}H line shapes observed in the 2D ^{1}H WISE NMR spectra confirmed that the high mobility of amorphous PEO was not imparted to the PC chains. More interestingly, the ^{1}H wide-line spectra recorded for neat PC showed clear spinning sidebands, in contrast to the spectra recorded for the polymer blends that were featureless (Figure 2 A). This revealed a bit surprising hindering of cooperative segmental motions of PC aromatic ring flips resulting from the mixing and interaction of basically rigid PC with highly mobile PEO.

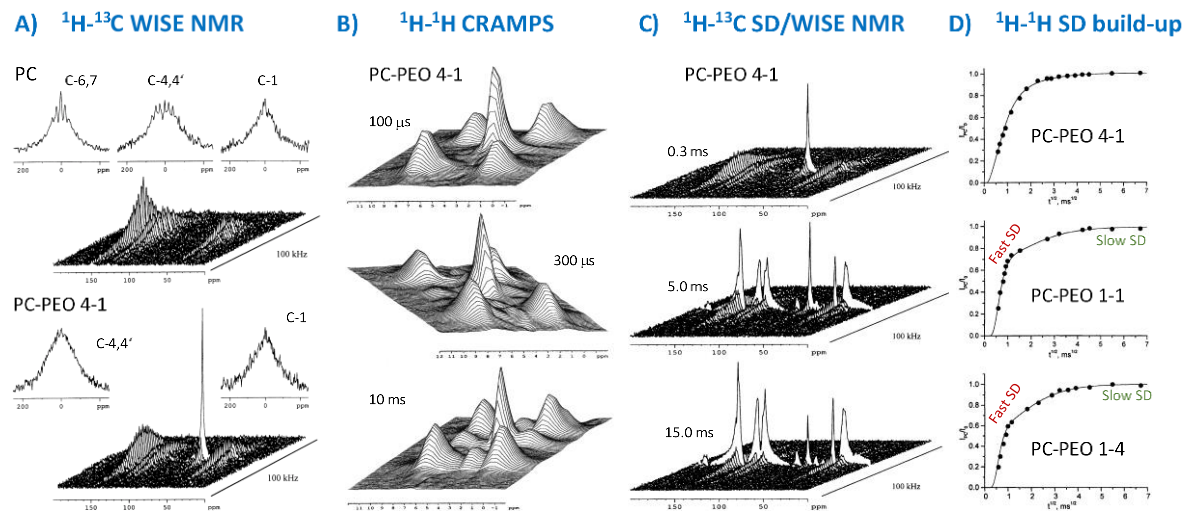

Figure 2. *^{1}H-^{13}C WISE spectra of neat PC and PC-PEO 4-1 blend (A); ^{1}H-^{1}H CRAMPS (B); and ^{1}H-^{13}C SD/WISE NMR spectra of PC-PEO 4-1 measured with variable spin-diffusion period (C); and ^{1}H-^{1}H spin-diffusion build-up curves (D).*

In order to gain a deeper insight into the distribution of the individual components, the ^{1}H-^{1}H spin diffusion was analyzed. As displayed in ^{1}H-^{1}H CRAMPS spectra (Figure 2B) the first cross-signals indicating dipolar interactions between PEO and PC units appeared within the 500-µs mixing time. This indicated an intimate mixing of both components in the amorphous phase. However, even after the 10-ms mixing time, the signals were not yet completely equilibrated.

The complex pathway of a multi-step ^{1}H spin-diffusion polarization transfer was then confirmed by the build-up dependences derived from 2D ^{1}H SD/WISE NMR spectra (Figure 2C, 2D). While the initial part of the build-ups reflected the ^{1}H polarization transfer in the amorphous phase, at longer times, the spin diffusion involved crystallites of PEO and PC. The careful simulation of these build-ups then allowed to estimate size of the domains of all components which were 0.3-0.8 nm in the amorphous phase, and 1.4-8.1 nm in the crystalline phase. In this way, we have been able to fully describe the architecture of the semi-crystalline polymer blends. *(For further details see the paper D1 included to the dissertation.)*

Our next research focused on the analysis of multi-step spin-diffusion processes, with the aim of tracing the interphase in polymer composites. In this context, we investigated composite networks consisting of polyimide and poly(dimethylsiloxane) chains (PI-PSX). Analysis of the ^{1}H-^{13}C WISE NMR spectra revealed not only nano-phase separation, but also two motional states of PSX chains. As deduced from the spin diffusion experiments, the surface of PSX domains is formed by a stiffened monolayer of short chains, while the fraction of more mobile PSX chains is located in the inner part of the domains. The determined domain sizes were then used to construct atomic-scale models, from which the molecular dynamics calculations quantitatively described the observed differences in the segmental dynamics (Figure 3A). *(For further details see the paper D2.)*

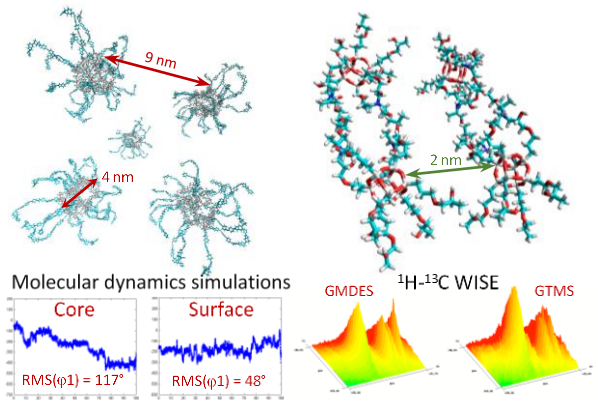

Figure 3. *Idealized models of PI-PSX networks (A), and epoxy-silica hybrids (B). Segmental dynamics of PSX chains is illustrated by the time dependence of Si-O-Si-O torsion angles, whereas the ^{1}H-^{13}C WISE spectra show segmental dynamics in epoxy-silica hybrids.*

The growing interest in organic-inorganic hybrids motivated us to focus on the surface structures of organically modified polysiloxane networks and silica particles. In this context, we have increasingly used quantum-chemical calculations to convert the ^{1}H-^{1}H spin diffusion data into the more reliable atomic resolution models. This way, four types of surface hydroxyls have been identified. These hydroxyls are not involved in rapid chemical exchange, nor do they form a homogeneous hydrogen bonding network, but rather form discrete nanometer-sized clusters the arrangement of which we have described. *(For further details see the paper D3.)*

This research gave us a deep insight into the interaction potential of silica-based fillers, which we later used to study complex behavior of hybrid organic/inorganic silica-epoxy films. In this research, the 2D ss-NMR experiments revealed a clear dependence between reaction conditions and the structure, segmental dynamics and self-organization of the synthesized films. Under the optimized conditions, the siloxane cage-like clusters were found to be regularly distributed throughout the bulk of the polymer matrix, when the inter-cluster distance, determined by spin diffusion experiments and SAXS, was about 1.8 nm (Figure 3B). Furthermore, a specific interaction between the silica surface and the polymer matrix was detected by the ^{1}H-^{29}Si HETCOR experiment. In this contribution we have found correlations between structural parameters and macroscopic properties. *(For the details see the paper D4 included to the dissertation.)*

2.3. Localization and distribution of water in biopolymers (D5, D6,)

The ^{1}H wide-line separation NMR experiments combined with the ^{1}H-^{1}H spin diffusion has not only received attention in probing heterogeneities in polymer composites, but this technique has also, found the application in the localization of water molecules in biological systems.[15] This application is based on a very simple idea: Water molecules tend to be more mobile than

the repeating units of biopolymers. Consequently, the corresponding ^{1}H wide-line spectrum of water is narrower than that of the biopolymer segments. Although H_2O cannot be detected directly in the ^{1}H-^{13}C WISE spectrum, the ^{1}H magnetization of water is encoded into the ^{13}C magnetization via the ^{1}H-^{13}C cross-polarization. This process can be further boosted by ^{1}H-^{1}H spin-diffusion transfer. This way, in the 2D ^{1}H-^{13}C WISE spectrum the narrow ^{1}H NMR signal of water can appear at ^{13}C resonance frequencies of the CH_x segments, which interact with water molecules. In order to enhance receptivity of this experiment the ^{1}H currier frequency is set *off ^{1}H resonance*. Using this set-up, a narrow well-resolved doublet appears in the corresponding ^{1}H wide-line spectrum.

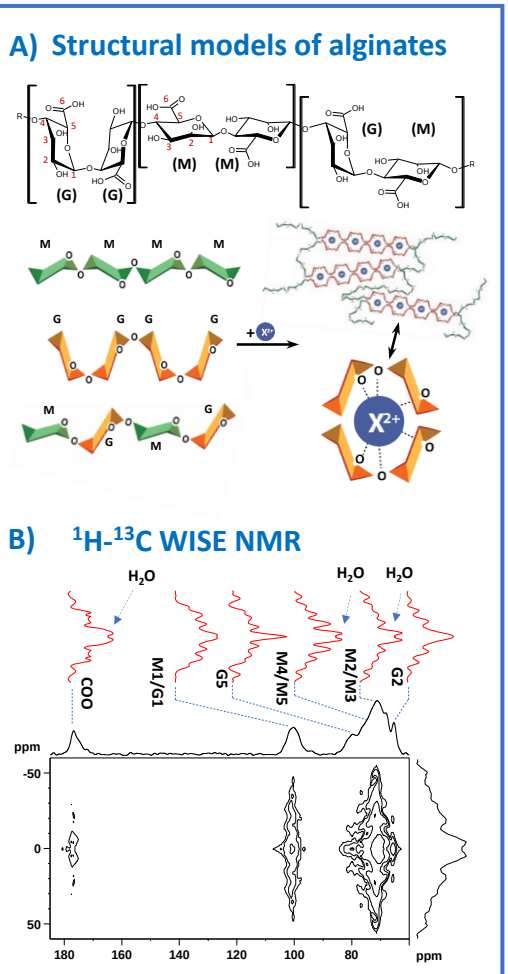

Figure 4. *Structural models of alginate macromolecules (A). ^{1}H off-resonance 2D ^{1}H-^{13}C WISE NMR spectrum of Al-alginate gel measured with 500 μs cross-polarization period (B).*

This approach we applied to gain a comprehensive insight into the atomic resolution structure and dynamics of polyvalent ion-crosslinked alginate gels in microbead formulations (Figure 4A). We revealed a two-component nature of the alginate gels, which results from the fluctuations in the concentration of residual water molecules that are preferentially localised in vicinity mannuronic acid (M) residues (Figure 4B). These hydrated M-rich blocks then tend to self-aggregate into sub-nanometre domains. In our later research, we described the interactions and structural transformations of the alginate gels in physiological environments simulating gastric and intestinal fluids and cellular environments. For these studies, we again used multinuclear ss-NMR spectroscopy, which identified a series of competitive ion-exchange and interconversion reactions, the rate of which depended strongly on the nature of the cross-linking metal ions. The experimental strategy presented in these studies thus provided a new perspective on the structure and dynamics of cross-linked polysaccharides (alginates) for which the high-quality atomic resolution diffraction data are unavailable. (*For further details see the papers D5 and D6 included to the dissertation*).

Altogether, the applied and optimized methodology based on the analysis of ^{1}H chemical shifts, ^{1}H wide-line spectra, ^{1}H-^{1}H dipolar interactions and spin diffusion, especially when combined with diffraction methods and quantum chemical calculations, has evolved into a robust strategy for the structural analysis of multicomponent heterogenous solids. This methodology has become an integral part of our approach, which we later used to develop domain-selective approaches of NMR crystallography and to study a wide range of polymer-based systems including *amphidynamic* materials (molecular machines) as well as composite pharmaceutical solids. (For example, see papers D7-D11 that are discussed in detail in later sections of the dissertation; Chapters 3, 4 and 5.)

3. ^{1}H-^{13}C Separation-Local-Field spectroscopy

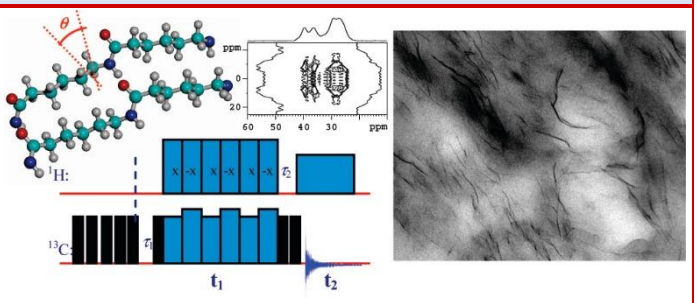

Due to the *multiple-spin* nature of the ^{1}H-^{1}H dipolar interactions the corresponding ^{1}H wide-line spectra provided only qualitative or semi-quantitative information about the segmental dynamics, while the details remained hidden. However, when simplified to the form of a ^{1}H-^{13}C *spin-pair* interaction, the corresponding dipolar profiles can be rigorously analysed in terms of geometric parameters. Therefore, we subsequently focused on the measurements of ^{1}H-^{13}C heteronuclear dipolar interactions with the aim of describing the local geometry of segmental motions in partially ordered nanocomposites. We have focused on the development and optimization of domain-selective modifications of the experimental techniques that allow the amplitudes of local fluctuations of molecular segments to be studied separately for individual domains in semicrystalline nanocomposites and *amphidynamic* polymer-based functional materials.

3.1. Introduction to the basics - Molecular dynamics in NMR spectroscopy

It has long been recognized that, in addition to the structure, molecular dynamics - on a wide range of timescales from picoseconds to seconds - determine the mechanical properties of polymers. In this context, the polymer chain dynamics exhibiting varying amplitudes and geometries, such as small-amplitude librations, aromatic ring flips or aliphatic side-chains jumps is characterized by an order parameter S^2 and a correlation time τ.

An insight into the correlation times is provided by spin-relaxation measurements, when segmental motions can be studied basically on two different time scales. The high-frequency (megahertz) motions are probed by the spin-lattice T_1 relaxation times measured in the laboratory reference frame, whereas the relaxation times measured in the rotating frame ($T_{1\rho}$) open the window into the mid-kilohertz motions. Briefly, the T_1 relaxation is the process of returning of a spin system to thermodynamic equilibrium during which the absorbed energy ($\Delta E=h\gamma B_0/2\pi$) is dissipated into the lattice as heat, and the part of macroscopic magnetization (M_z) that is parallel with the direction of the static magnetic field (B_0) decays exponentially. The recovery of macroscopic magnetization is driven by local fluctuations which frequencies are close to the resonance frequency of a given nucleus. Consequently, measurements of T_1 relaxation times of various nuclei cover a wide range of motion frequencies from tens to hundreds of MHz. The analysis of low-frequency motions then requires the application of much weaker magnetic fields, which is experimentally achieved by applying the spin-locking B_1 fields in the rotating frame, the intensities of which are ranging from ca. 10 to 100 kHz.

The order parameter S^2 is a measure of the equilibrium distribution of orientations of the bond vector μ(t) in a molecular reference frame and ranges from 1 for fixed orientation to 0 for free motion.[16] In the simplest case, assuming a small-amplitude (θ) axially-symmetric motion, the order parameter can be converted[16-18] to the average fluctuation angle $\sqrt{\langle\theta^2\rangle}$:

$$S^2 = 1 - \frac{3}{2}\langle\theta^2\rangle \qquad (1)$$

For more complex motions, other models providing more informative pictures can be used. For example, fast jumps of the bond vector between N distinct orientations with populations p_i are described using to the following relationship[16,18]:

$$S^2 = \sum_{i,j=1}^{N} p_i p_j P_2(cos\theta_{ij}) \qquad (2)$$

And one of the most elegant way of determining the order parameters is the measurement of the spin-pair ^{1}H-^{13}C dipolar interactions in CH or CH_2 segments.

3.2. Measurement of heteronuclear $^1H–^{13}C$ dipolar couplings (D12)

The magnitude of the heteronuclear $^1H–^{13}C$ dipolar interactions is naturally encoded in the signal build-up during the $^1H–^{13}C$ cross polarization (CP). Unfortunately, the application of traditional on-resonance ^1H and ^{13}C spin-locking fields does not provide detailed information. This is because the ^1H-^1H dipolar interactions are still active and due to the fast ^1H spin diffusion the CP build-up dependencies are averaged and smoothed.

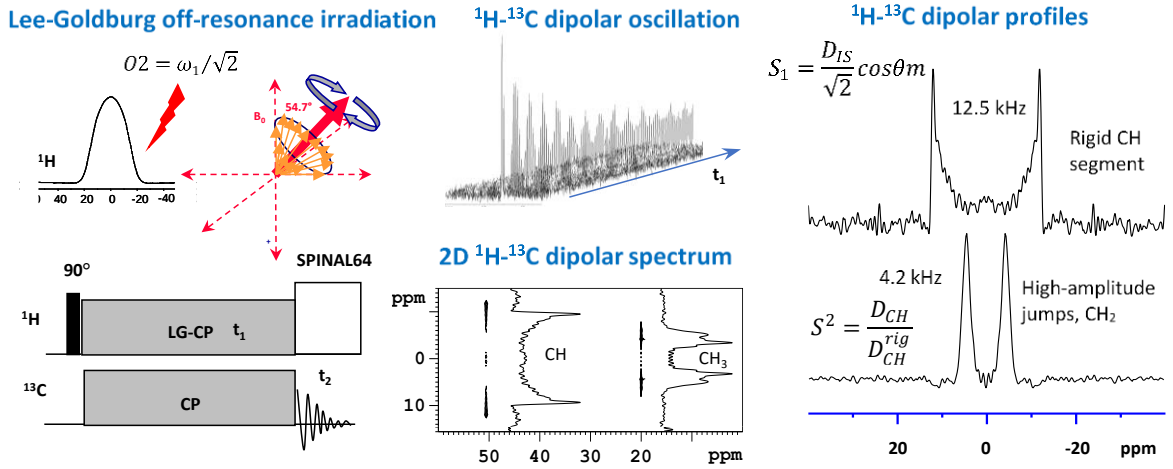

Figure 5. *Schematic representation of Lee-Goldburg off-resonance cross-polarization; ^1H-^{13}C dipolar oscillation observed during LG-CP; 2D ^1H-^{13}C dipolar NMR spectrum of alanine; and ^1H-^{13}C dipolar profiles separated for rigid CH segments and CH_2 groups executing high-amplitude jumps.*

However, when the ^1H-^1H dipolar interactions are suppressed by using the off-resonance Lee-Goldburg spin-locking, when the ^1H spins are aligned along the B_1 tilted by 54.7° with respect to the static magnetic field, the $^1H–^{13}C$ dipolar oscillations are reestablished (Figure 5). Fourier transformation of this oscillation then provides the dipolar spectrum which reflects an effective $^1H–^{13}C$ dipolar coupling constant. In the 2D arrangement the dipolar spectra are separated for each molecular segment according to the ^{13}C NMR chemical shift (Figure 5). The order parameter S^2 then can be determined from these dipolar profiles. This is because any molecular motion with a correlation time less than ca. 40 μs causes averaging of one-bond $^1H–^{13}C$ dipolar coupling. The ratio of a motionally averaged dipolar coupling constant (D_{CH}) and the rigid-limit value ($D_{CH,rig}$) defines the order parameter S^2 (Figure 5) that can be converted to the amplitude of segmental motion using the above-introduced relations.

Following this idea, a number of experimental *dipolar recoupling* separation-local-field (SLF) techniques with improved sensitivity such as PILGRIM or

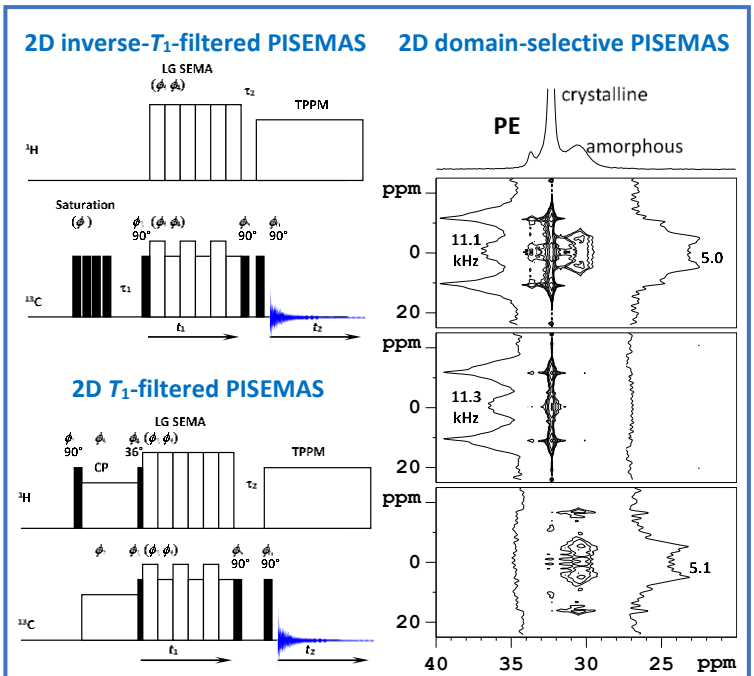

Figure 6. *The inverse-T_1-filtered and T_1-filtered PISEMAS experiments selecting coherences in amorphous and coherence phase only; the corresponding ^1H-^{13}C domain-selective PISEMAS dipolar spectra of semi-crystalline PE.*

PISEMAS have been developed and applied to study the segmental dynamics of a wide range of organic, bioorganic and hybrid solids.[19,20] Unfortunately, polymer nanocomposites and multicomponent solids are often semi-crystalline systems producing complex and overlapped NMR spectra with a poor dispersion of the signals in isotropic ^{13}C dimension. Although the segmental dynamics of the polymer chains in the crystalline and amorphous phase is different, the limited spectral resolution causes a detection of distorted dipolar profiles reflecting an envelope of a wide range of motionally averaged dipolar couplings. Consequently, an accurate analysis of the segmental dynamics requires the measurement of the dipolar spectra for each polymer segment separately in amorphous and crystalline phases.

For such task we have developed and optimized several PISEMA-based pulse sequences. Just for illustration, the selection of the ^{13}C magnetization originating from only the amorphous phase was achieved by an *inverse-T_1-filter*; i.e. a train of saturation pulses followed by a short delay and a direct excitation ^{13}C pulse. Dipolar oscillation was then initiated by the frequency- and amplitude-switched "reverse" LG $^{13}C \rightarrow {}^{1}H$ cross-polarization. This way, also the evolution of an unwanted net ^{13}C magnetization was prevented (Figure 6, left upper sequence). In contrast, by placing the *direct T_1 relaxation filter* after the recoupling block the dipolar spectra are selected for the crystalline components only. The efficiency of the coherence selection and recoupling of the heteronuclear dipolar couplings was documented on several systems such as semicrystalline polyethylene (PE) (Figure 6, right). (*For further details see the paper D12 which included to the dissertation*).

3.3. Amplitudes of local motions in polymeric nanocomposites (D7, D13)

Later, we applied the developed domain-selective *inverse-T_1-filtered* and *T_1-filtered PISEMAS* experiments to investigate thermomechanical properties and polymer chain dynamics in multi-component semi-crystalline polymeric materials. Typical examples of these multiphase systems are nanocomposites based on polyamide-6 and montmorillonite (MMT), where a significant improvement in toughness and elongation at break has been achieved by co-adding a small amount of ethylene-methyl acrylate copolymer (EMA, 5 wt. %). To investigate the observed changes in the three-component system, the motional behavior of the polymer segments was studied using the developed 2D PISEMAS-based ^{1}H-^{13}C dipolar recoupling techniques. Measurements made separately in amorphous and crystalline domains (Figure 7) have allowed a large collection of high quality site-specific dipolar profiles to be analyzed with respect to the distribution of motion amplitudes. This way it was found out that in α- and γ- crystal modifications of PA6 as well as in the "constrained" domains of the amorphous phase of PA6 the amplitudes of rotational-diffusion motion of CH_2 groups (10°-33°) increase from NH and CO groups toward the central part of the repeating units. When comparing both crystal modifications it was shown that less tight packing of polymer chains in γ-form increases fluctuation angle by about 5°.

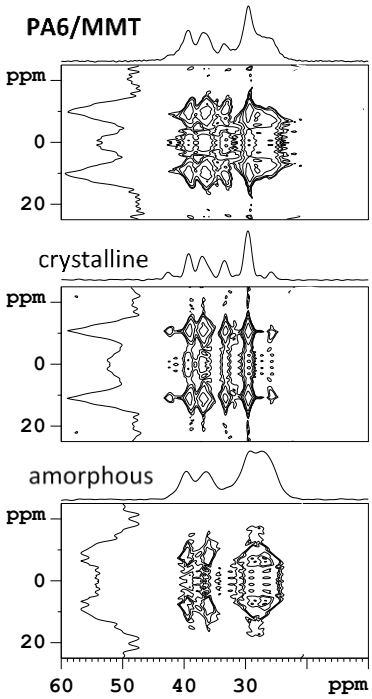

Figure 7. *The ^{1}H-^{13}C domain-selective PISEMAS dipolar spectra of a semi-crystalline PA6/MMT system.*

A bit counterintuitively, the dipolar profiles also revealed that the presence of silicate platelets in amorphous PA6 matrix enhances motional amplitudes of polymer segments in nanocomposites. This fact supports the explanation that fast and relatively small-amplitude motions occurring in the glassy state of PA6 can be considered as mechanically active and as a potential additional factor that may help to enable the larger amplitude motions (jumps) associated with the glass transition temperature. Finally, the increase in ductility observed in the triple-component system was

attributed to the formation of EMA copolymer domains surrounded by clay platelets. The polymer chains in these fully phase-separated domains exhibit large amplitude motions. (For further details see the paper D13 included to the dissertation).

Moving on to more complex nanostructured materials with hierarchical architecture, we then focused on epoxy networks based on poly(propylene oxide) chains cross-linked with diglycidyl ether of bisphenol A, additionally reinforced with polyhedral oligomeric silsesquioxanes (POSS). Molecular dynamics studies, carried out using a variety of 'domain-selective' experiments, provided information that allowed the contribution of molecular segments to be assigned to thermomechanical properties such as T_g and storage shear modulus, as well as predicting the ability of individual components to absorb mechanical energy. Remarkable motion heterogeneities were found not only in the amorphous phase, where the mobile polymer segments of the "free" domains coexist with the immobilized chains of the "constrained" ones, but also in the crystallites of POSS building blocks, where the large-amplitude segmental reorientations in the mid-kilohertz frequency range were identified. For instance, in the $POSS_{Ph}$ crystallites the two-site 180° flips accompanied by the 25° wobbling of the flip axes dominate to aromatic rings (Figure 8). Similarly, cyclopentyl substituents in $POSS_{Cp}$ crystalline domains were found to execute ca. 35° rotational-diffusion motion. (*For the details see the paper D7 included to the dissertation*).

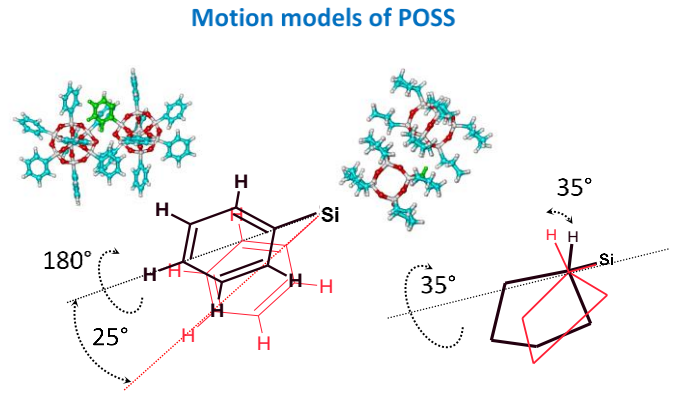

Figure 8. *Schematic representation of segmental motions in the crystallites of $POSS_{Ph}$ (left) and $POSS_{Cp}$ units (right).*

3.4. Metallacarborane nanorotors in polymer matrices (D8, D9, D14)

Solids that combine long-range order with rapid molecular reorientation offer a promising approach to the development of a new class of functional materials called as *molecular machines*. The power of dipolar SLF NMR spectroscopy is then best illustrated by our studies of *amphidynamic* systems that resemble molecular machines, where certain molecular segments perform well-defined high-amplitude motions, while the other parts represent a stator with the sites accessible for specific non-covalent molecular interactions.[21,22]

In this context, metallacarboranes, as bulky compounds with delocalized charge, represent a unique class of building blocks for the synthesis of *amphidynamic* systems.[23-25] To demonstrate this capability different nanocomposites based on dicarbollide ions (CoD^-) incorporated into the poly(ethylene oxide) (PEO), and poly(vinyl pyridine) matrices were synthesized. It was found out that the interaction of neutral PEO with CoD^- ions driven by weak dihydrogen bonding resulted in the formation of a uniquely organized periodic structure. In spite of crystalline-like molecular arrangement, the CoD^- ions exhibited uniaxial large-amplitude rotational motions over the broad range of temperatures. Macromolecules thus represented a rigid support (stator) for the more mobile CoD^- ions (rotators). The obtained findings also revealed that a relatively simple procedure could be used for the preparation of well-defined *amphidynamic* nanocomposites, thereby opening a route to construct sophisticated supramolecular systems. (*For the details see papers D8 and D9 included to the dissertation*).

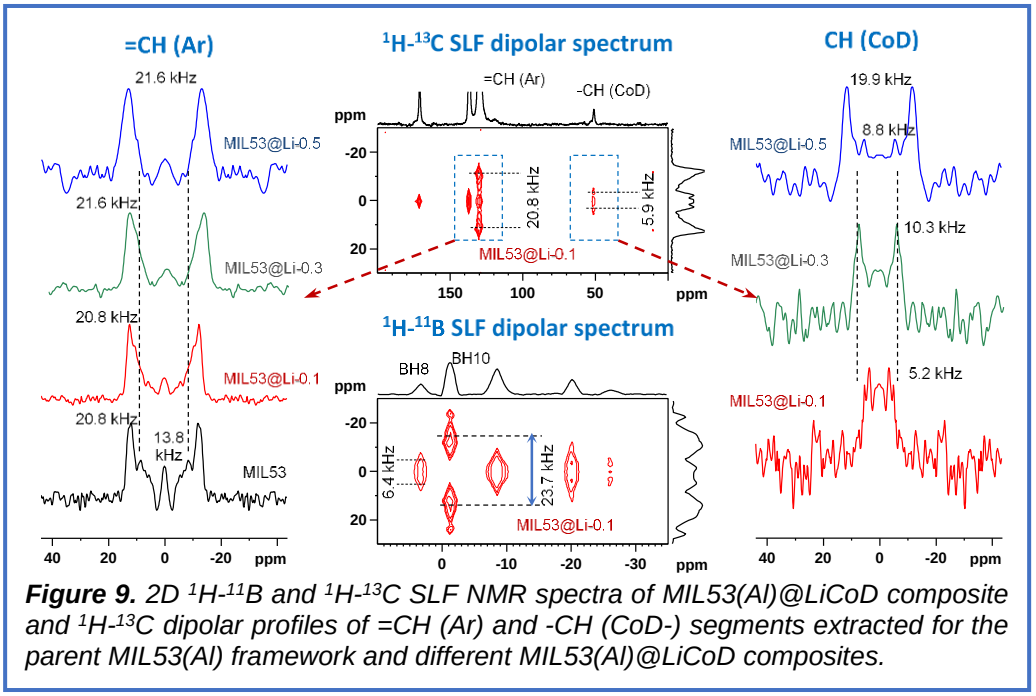

Figure 9. *2D ^{1}H-^{11}B and ^{1}H-^{13}C SLF NMR spectra of MIL53(Al)@LiCoD composite and ^{1}H-^{13}C dipolar profiles of =CH (Ar) and -CH (CoD-) segments extracted for the parent MIL53(Al) framework and different MIL53(Al)@LiCoD composites.*

Last but not least, the detailed analysis of ^{1}H-^{13}C and ^{1}H-^{11}B SLF dipolar experiments (Figure 9) has given us an insight into the dynamics of composite materials for *all-solid-state* electrolytes based on the MIL53(Al) metal-organic-framework featuring metallacarborane (Li^+CoD^-) ions. Although the framework channels are relatively narrow (ca. 10-11 Å, Figure 10), the incorporated CoD^- ions execute a uniaxial high-amplitude 5-fold jumps along the main symmetry axis defined by B10 boron atoms (Figure 10). The aromatic linkers of MOF then undergo medium-amplitude angular fluctuations of ca. 15°. However, the inner doublet in ^{1}H-^{13}C dipolar spectrum, with a splitting of ca. 13.8 kHz (Figure 9, left column), shows the coexistence of a minor fraction of aromatic linkers/rings executing the high-amplitude 180° flips. (*Further details can be found in paper D14 included to the dissertation*).

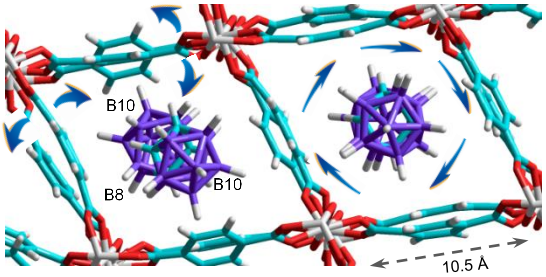

Figure 10. *Schematic representation of segmental motions in the MIL53(Al)@LiCoD composite.*

The separation-local-fields (SLF) NMR experiments, which allow the measurement of motion-averaged site-specific heteronuclear one-bond ^{1}H-X dipolar coupling constants, are currently standard instruments providing an insight into the geometry, amplitudes and constrains of local segmental motions in a wide range of even very complex molecular solids. For example, we have successfully applied this experimental strategy to understand phase transformations in biopolymers (D5), to describe the physical state of organic phases incorporated into mesoporous silica particles (D15), or to fully unravel the hidden processes associated with the polymorphic changes in some active pharmaceutical ingredients.[26] Based on a detailed description of the thermal activity of the high-amplitude motions, it has been possible to explain at atomic resolution not only changes in the thermomechanical properties of many polymer systems, but also to gain insight into the mechanism of many physicochemical processes, such as ionic conductivity in all-solid-state electrolytes (D14). Thus, in the field of advanced high performance ss-NMR spectroscopy of multicomponent solids, the SLF NMR experiments play an important role.

4. 2D correlation spectroscopy of quadrupolar nuclei

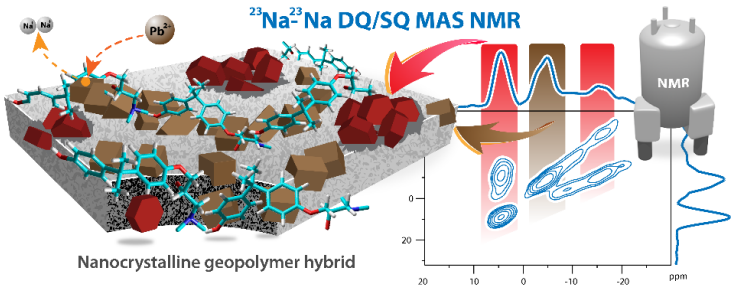

As we entered the world of functional, energy-related and construction materials, it became clear that a key to their structural analysis holds the resonance frequencies of quadrupolar nuclei such as ^{11}B, ^{7}Li, ^{23}Na or ^{27}Al. And thus, we have also focused on 2D correlation techniques involving quadrupolar nucley supported by DFT calculations in order to monitore the covalent and non-covalent assembly of individual bulding blocks. In this way, for instance, we discovered the previously unreported boroxine structures stabilized by a secondary coordination. Further, by combining double-quantum (DQ) MAS NMR correlation spectra, systematic analysis of DQ build-up dependences and quantum chemical calculations, we explained specific interactions in a novel type of ion-conducting materials, described the local structure and distribution of cross-links in boron-modified phenol-formaldehyde resins for soft magnetic composites, and understood the interface-induced growth of polymer-conjugated proto-crystalline phases in aluminosilicate hybrids and geopolymers.

4.1. Introduction to the basics - The "glory" and "misery" of quadrupolar nuclei

When looking at the periodic table it is clear that the most abundant NMR active nuclei (isotopes) are the nuclei with a nuclear spin larger than ½. These nuclei (more than 70 % of all NMR active nuclei) are called as quadrupolar, possess an integer (I=1 or 3) or half-integer nuclear spin (I=3/2, 5/2, 7/2 or 9/2), and are widely distributed in living and non-living nature.

As given by the Zeeman interaction ($\hat{H}_Z$), the advantage of ½-spin nuclei arises from the fact that these nuclei can exist in two main energy states (levels), and because during the ss-NMR experiment we observe coherent transitions between these levels, the resulting NMR spectra display symmetrical single lines influenced by relatively weak interactions such as chemical shift ($\hat{H}_{CS}$) and dipolar interactions ($\hat{H}_{DD}$), the anisotropy parts of which are effectively removed by MAS and dipolar decoupling. Scalar interactions ($\hat{H}_J$) are usually neglected in the solid state. In contrast, the quadrupolar nature of the nuclei with I > ½ greatly complicates the analysis of corresponding ss-NMR spectra. The reason for this is the fact that these nuclei can exist on several energetic levels (Figure 11, central upper panel) and have non-spherical charge distribution. The nuclear spin then interacts with the electric field gradient, which leads to quadrupolar splitting of the NMR signal, sometimes reaching up to tens of MHz. Quadrupolar interactions ($\hat{H}_Q$) are strong enough to cause dramatic broadening of the detected signals (Figure 11, left upper panel, the black spectrum).

In contrast to chemical shift anisotropy and dipolar interactions, the suppression of quadrupolar interactions is much more complicated. According to the perturbation theory, the quadrupolar interaction can be divided into two contributions, quadrupolar splitting of the first ($\hat{H}_Q^1$) and second order ($\hat{H}_Q^2$). The spatial portion of these energy contributions can be further described as spherical harmonic oscillations P_2 and P_4 (Figure 11, right upper panel):

$$\hat{H}_Q^1: P_2(\cos\chi) = \tfrac{1}{2}(\cos^2\chi - 1) \quad (3)$$

$$\hat{H}_Q^2: P_4(\cos\chi) = \tfrac{1}{8}(35\cos^4\chi - 30\cos^2\chi + 3) \quad (4)$$

where χ represents the angle between the main axis of quadrupolar interaction tensor and the direction of the static magnetic field. Equations (3) and (4) indicate how the quadrupolar interactions of the 1st and the 2nd order can be eliminated. Here, the 1st order quadrupolar interaction is equivalent to the chemical shift anisotropy. This means that the spherical harmonic oscillation P_2 becomes equal to 0 and the corresponding part of the 1st order

quadrupolar interaction vanishes, when MAS is applied (i.e. when the rotation axis holds an angle of 54.7° and the rotation frequency is high enough > 10-20 kHz) (Figure 11, right upper panel, green line). Although the resulting spectrum is significantly narrowed to ca. ⅓ of the original width (Figure 11, left upper panel, the red spectrum), the contribution of the 2nd order quadrupolar interaction is still present. As described by the harmonic oscillation P_4, this contribution is suppressed by rotating the sample at an angle of 30.56° or 70.12°. This means that to remove the influence of the quadrupolar interaction completely, the sample must be rotated around several axes simultaneously. And following this finding two different experimental approaches, known as double rotation (DOR) and dynamic angle spinning (DAS) have been proposed (Figure 11, left bottom panel).[27-30]

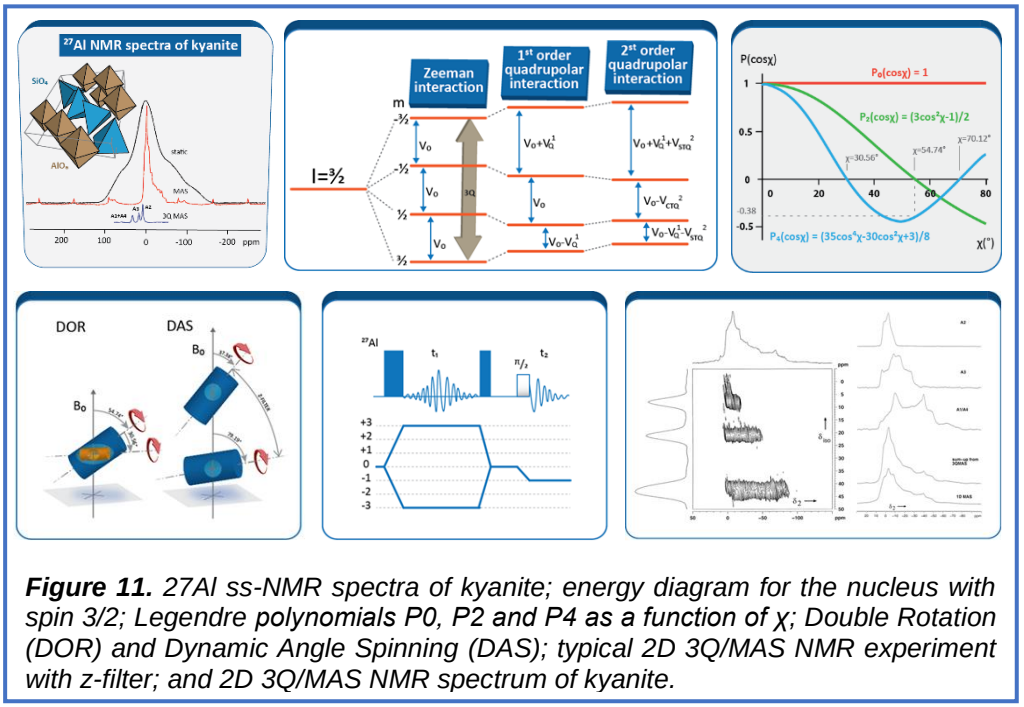

Figure 11. *27Al ss-NMR spectra of kyanite; energy diagram for the nucleus with spin 3/2; Legendre polynomials P0, P2 and P4 as a function of χ; Double Rotation (DOR) and Dynamic Angle Spinning (DAS); typical 2D 3Q/MAS NMR experiment with z-filter; and 2D 3Q/MAS NMR spectrum of kyanite.*

However, both techniques require a special design of measurement probe-heads. Therefore, an alternative concept has been developed. Instead of complicated mechanical manipulation of the sample, the nuclear spins are manipulated in spin space by strong *rf* pulses (Figure 11, central bottom panel). This concept is based on the excitation and evolution of triple quantum coherence (3QC) and basically provides the same type of information as the previously mentioned dynamic angle experiments. In a typical 3Q/MAS NMR experiment, a large amount of triple-quantum coherence is generated by the first, very strong *rf* pulse (Figure 11, central bottom panel).[31,32] This 3Q coherence subsequently evolves during the t_1 detection period with a frequency that corresponds to the triple frequency of isotropic chemical shift ($3\times\omega_{cs}$) and $^{6}/_{4}$ frequency of the 2nd-order quadrupolar interaction ($^{6}/_{4}\times\omega_{Q}^{2}$). In the end of this period, the 3Q coherence is transferred back to the observable single-quantum coherence (1Q). This coherence then evolves in the opposite direction with the frequency corresponding to the unscaled isotropic chemical shift ($1\times\omega_{cs}$) and the 2nd-order quadrupolar interaction ($1\times\omega_{Q}^{2}$). In the resulting 2D spectrum then the isotropic chemical shift is stored in dimension (F_1), while the quadrupolar broadening is separated in the dimension (F_2). Consequently, individual sites can be easily resolved and identified in F_1 dimension. The real potential of this 2D experiment is shown in Figure 11, right bottom panel, where 3 different sites of kyanite can be identified. Further details can be found in our previous articles.[33,34]

The MQ/MAS NMR technique has been further developed, toward the highest resolution and sensitivity as possible.[35-37] Consequently, the analysis of ss-NMR spectra of quadrupolar nuclei has become a standard element in the structural analysis, opening thus avenues for new structural discoveries in inorganic materials and organic-inorganic hybrids.

4.2. Boron atoms as coordination centers (D16, D17)

The information comprehensiveness and richness of quadrupolar nuclei NMR spectra, especially when advanced 2D multiple-quantum ^{11}B–^{11}B MAS NMR techniques are combined with the quantum chemical geometry optimizations is well illustrated by our investigation of the structure and arrangement of cross-linking units in boron-modified phenol–formaldehyde resins. The analysis of ^{11}B ss-NMR spectra based on the quantum-chemical calculation of NMR parameters performed for a representative set of model structures then attributed the boron-based cross-links to the monoester and diester six-membered spirocyclic borate anions with tetrahedral coordination (Figure 12). The ^{11}B–^{11}B double-quantum correlation MAS NMR experiments[38] then revealed that a non-negligible fraction of the spirocyclic borate complexes existed in pairs or small clusters, in which the average ^{11}B···^{11}B interatomic distance was less than 5.5 Å. Our systematic study thus clearly confirmed receptivity of relatively weakly resolved ^{11}B ss-NMR spectra to even very tiny changes in local coordination geometry, and further demonstrated the reliability of high-level quantum-chemical calculations. (For further details see the paper D16 included to the dissertation).

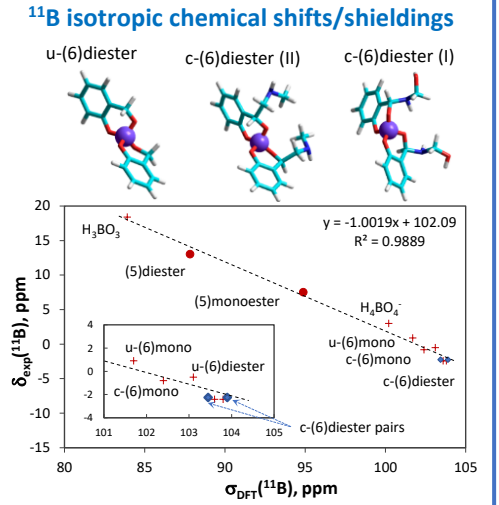

Figure 12. *Optimized geometries of cross-linking units in boron-modified phenol–formaldehyde resins; and experimental ^{11}B isotropic chemical shifts with their corresponding isotropic chemical shieldings.*

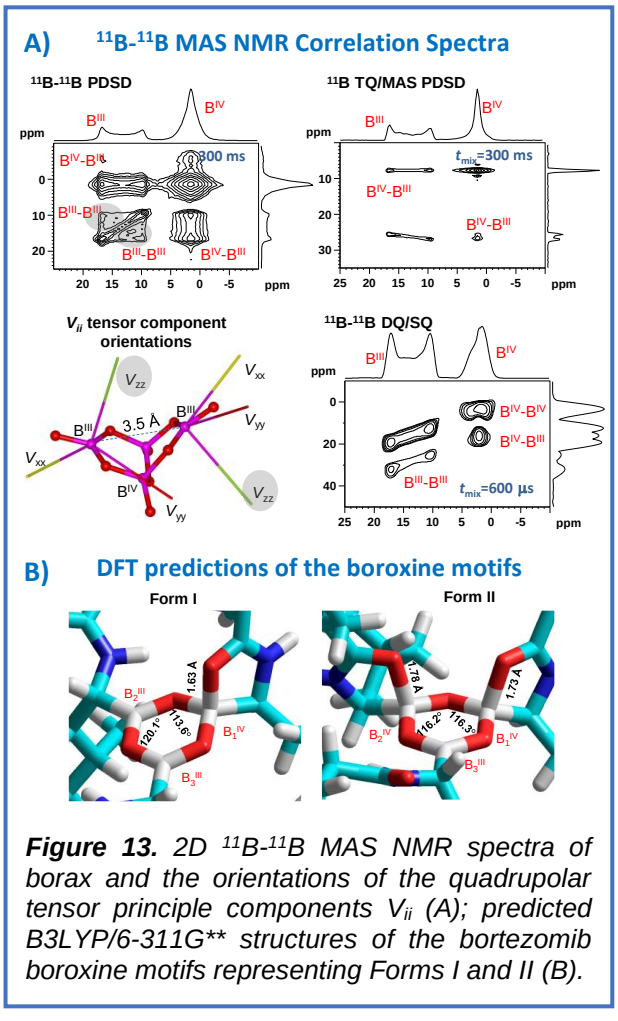

Figure 13. *2D ^{11}B-^{11}B MAS NMR spectra of borax and the orientations of the quadrupolar tensor principle components V_{ii} (A); predicted B3LYP/6-311G** structures of the bortezomib boroxine motifs representing Forms I and II (B).*

Full potential of NMR spectroscopy of quadrupolar nuclei was then utilized later, when we explored various 2D ^{11}B-^{11}B ss-NMR correlation techniques (Figure 13A) combined with DFT calculations to investigate the assembly process of boronic acid residues in the solid state. This way, we discovered unique, previously unreported boroxine structures exhibiting secondary coordination. A uniform distance in ^{11}B-^{11}B spin pairs was conclusively deciphered by the through-space ^{11}B-^{11}B double-quantum (DQ) coherence build-ups, whereas the distinct 2D ^{11}B-^{11}B DQ correlation patterns revealed several unique boroxine structures differing in their local geometries. The boroxine rings were found to be internally stabilized by the transformation of the trigonal boron sites to the tetrahedral geometry, when the secondary five-membered rings were formed (Figure 13B). It was thus confirmed that ^{11}B NMR parameters respond sensitively to subtle

changes in the local geometries, which can be reliably interpreted and visualized by DFT calculations. This has led to the development of an efficient strategy for exploring the assembly of boronic acid derivatives. (*For the details see the paper D17, which is included to the dissertation*).

4.3. Lithium ion transfer in polymer electrolytes (D14, D18-D20)

The previously achieved knowledge and methodological experiences in the field of NMR spectroscopy of quadrupolar nuclei were further utilized in the research of Li-ion conductivity of polymeric and *all-solid-state* electrolytes. In this context we focused on the development and characterization of a new category of ion-conducting materials based on an MIL53(Al) framework with incorporated metallacarborane (Li^+CoD^-) ions. Besides the local dynamics of metallacarborane clusters and polymer segments as discussed above in Chapter 3.4. we particularly focused on describing the interactions and mobility of Li^+ ions. Bear in mind that ^{7}Li and ^{27}Al are quadrupolar nuclei with I = 3/2 and 5/2, respectively. By analyzing the ^{27}Al and ^{7}Li ss-NMR spectra, the MIL53(Al)@LiCoD framework was found to adopt predominantly an open-pore conformation accompanied by a minor fraction of narrow-pore channels. The inserted Li^+ ions have been found in two states (free and bound), which both exhibit remarkable motions. The recorded 2D ^{7}Li–^{7}Li DQ/SQ NMR spectra then showed well-evolved autocorrelation *free–free* and *bound–bound* signals, which revealed the formation of chains of lithium ions of the same type. At the same time, by analyzing the ^{7}Li-^{7}Li DQC build-ups, it was possible to estimate the average Li^+...Li^+ distances. It is worth noting that the calibration of ^{7}Li-^{7}Li DQC build-ups (Figure 14, left upper graph) was performed using the data previously obtained for the ^{11}B-^{11}B interatomic distances. (Figure 14, left bottom graph) [ref D17]. Both types of Li^+ ions were found in the slow mutual chemical exchange (Figure 14) and forming the chains, which are large enough to enable efficient long-range charge transfer and macroscopic conductivity. (*For further details see the paper D14 attached to the thesis*).

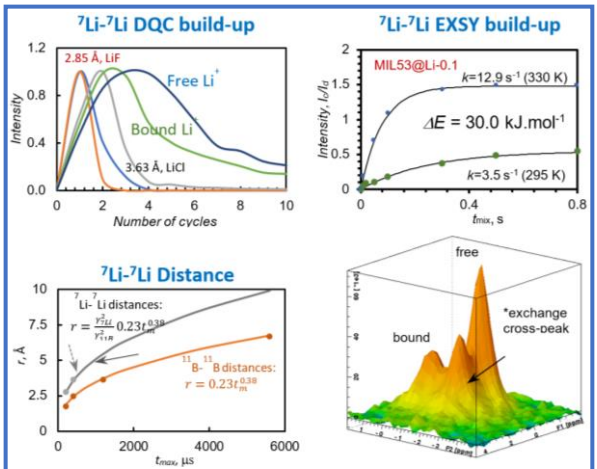

Figure 14. *^{7}Li-^{7}Li DQC build-up dependences; the dependences between the t_{max} recoupling time and interatomic distances for ^{11}B and ^{7}Li spins; ^{7}Li-^{7}Li EXSY build-up dependences and a typical ^{7}Li-^{7}Li EXSY NMR spectrum.*

In the context of structural analysis of energy-related materials and polymeric electrolytes,[39] and using the same or similar methodological approach, we have investigated the structural transformation in fluoroethylene carbonate-containing $LiPF_6$ electrolytes [D18], Li-ion mobility in polynorbornene-based polyelectrolytes with covalently attached metallacarboranes [D19], and garnet-poly(ε-caprolactone-co-trimethylene carbonate) polymer-in-ceramic composite electrolytes for all-solid-state lithium-ion batteries [D20]. (*For further details, see papers D18-D20 that are attached to the thesis*).

4.4. Structural transformations in aluminosilicate solids (D21-D23)

Another typical example of solid systems the structural characterization of which relies on NMR spectroscopy of quadrupolar nuclei are aluminosilicate framework materials – zeolites, and their amorphous analogues – geopolymers.[33,40,41] The structural complexity of these systems,

for which the coexistence of multiple phases including amorphous, partially ordered and crystalline domains is a typical feature, results in the wide distribution of NMR parameters whose origin is difficult to decipher.[42] Consequently, a detailed insight into the local structure of these systems requires the application of special techniques that allow NMR spectra to be manipulated and appropriately *edited*. Typically, we applied this *domain-edited* approach to clarify the problem of undesired crystallization of aluminosilicate polymers (AIPs, geopolymers) that is accompanied by the loss of mechanical strength. The application of ^{27}Al MQ/MAS NMR and {^{1}H}-REDOR-^{27}Al MQ/MAS NMR spectroscopies, combined with the biaxial shearing transformations, then elucidated the structural basis of this behavior, when the destabilization of AIPs was found to be associated with the presence of bridging hydroxyl groups (Si–OH^{+}–Al, Brønsted-acid sites) that induce breaking of Si–O–Al bonds. (*For further details see the paper D21 attached to the thesis*).

Further we focused on the structural characterization of aluminosilicate hybrids with polymer-conjugated nanosized zeolite fractions. The 2D ^{23}Na–^{23}Na DQ MAS NMR spectra revealed the existence of sites the local geometry of which allows for the pairing of sodium ions (Figure 15, right). Consequently, these sites are accessible and suitable for the exchange with Pb^{2+} ions, suggesting thus a route for the preparation of a novel type of geopolymers capable for capturing metal cations. (*For further details see the paper D22 attached to the thesis*).

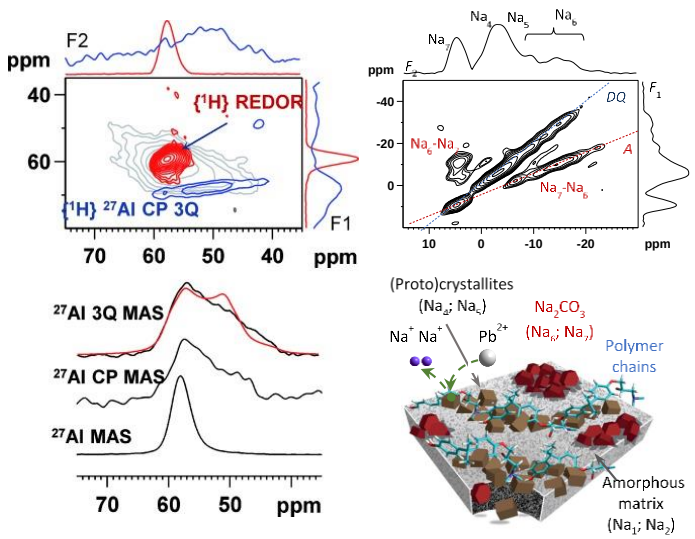

Figure 15. *Domain-edited ^{27}Al MQ/MAS NMR spectra and the F_1 and F_2 projections of the hydrated Ca-CHA zeolite (left); ^{23}Na-^{23}Na DQ/MAS NMR spectrum and the model of the hybrid geopolymer (right).*

In the same period, we extended this approach by applying the {^{1}H}-^{27}Al CP/MQ/MAS NMR technique and DFT/MM calculations (Figure 15, left). This way in zeolites, we were able to identify not only Brønsted Si(OH)Al acid sites, but also framework protonated Al_{FR} Lewis acid sites as well as dehydroxylated $(SiO)_3Al$ Lewis sites which exhibited *extremely* broad ^{27}Al NMR resonances. (*Details of this research are summarized in the paper D23 attached to the thesis*).

Thus, it is clear that the advanced ss-NMR spectroscopy of quadrupolar nuclei, which allows to extract NMR parameters with a high-precision, combined with quantum-chemical calculations, provided a detailed atomic resolution insight into the mechanism of many physicochemical processes, such as ionic conductivity, metal sorption ability or catalytic activity. The knowledge obtained using these experimental techniques and strategies are paving currently the way for the design of the next generation of catalysts, construction and energy-related materials.

5. Toward the domain-edited NMR crystallography

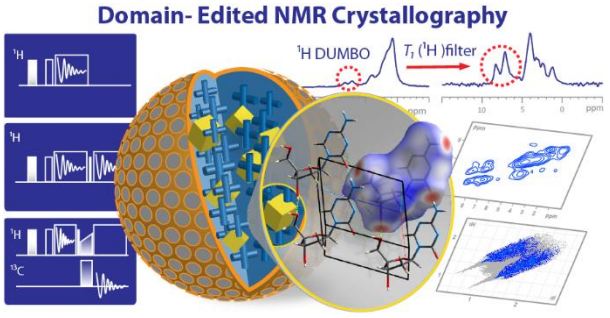

The experimental techniques and approaches described above have been synergistically combined for the structural characterization of polymer-based drug delivery systems in which the active ingredients are embedded in the polymer matrix. Precise structural analysis of these multiphase systems, which is a stringent requirement for their therapeutic applications however, remains a challenge. The presence of multiple components and phases results in complicated spectroscopic (diffraction) patterns, the conversion of which into the refined structures is practically unattainable. Therefore, we have explored a combination of various ss-NMR techniques with DFT calculations and data processing to formulate a general experimental-computational strategy providing inside into these multipotent solids at atomic resolution level.

5.1. Structural diversity of solid polymeric dispersions (D10, D11, D24)

The concept of *solid dispersions* (SDs) to enhance the absorption of poorly water-soluble is based on dispersing a hydrophobic active pharmaceutical ingredient (API) into a hydrophilic nontoxic matrix.[43] SDs are also important during early stage drug development because they maximize drug exposure during animal experimentation. Solid dispersions can also reduce the dissolution rate of highly soluble drugs, generating thus promising controlled-drug-release systems. Despite extensive research, applications of pharmaceutical solid dispersions have remained limited. This follows from the fact that SDs are structurally very complex materials. As their synthesis is controlled by a combination of thermodynamic and kinetic factors, we currently distinguish more than 15 types of SDs, the reliable structural characterization of which is extremely challenging.[44]

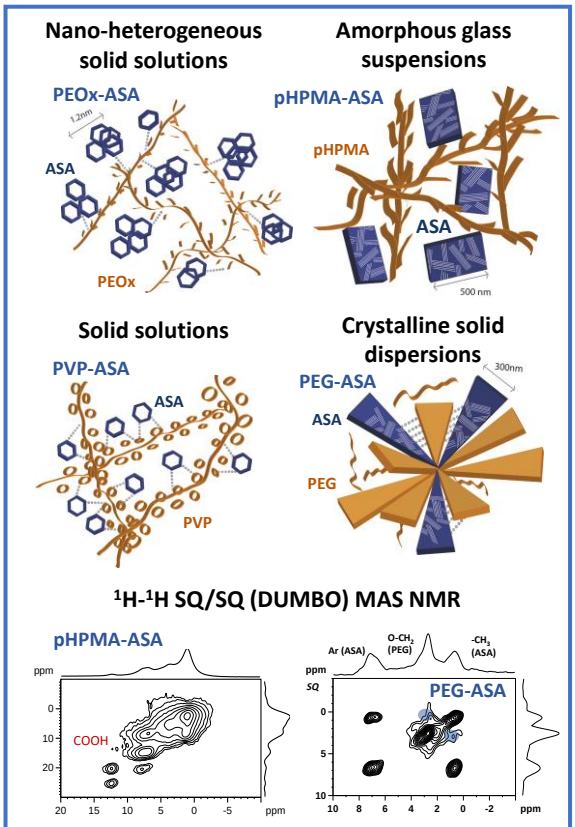

Figure 16. *Schematic representation of distinct types of polymer–ASA solid dispersions; and typical 2D ^1H–^1H SQ/SQ DUMBO NMR spectra (10 kHz).*

To explore this field of structural analysis and to optimize experimental procedure how to reliably identify individual types of solid dispersions we prepared by a freeze-drying method various types of solid dispersions of acetylsalicylic acid (ASA) in PVP, pHPMA, PEOx, and PEG. By combining DSC, WAXS, ^{13}C CP/MAS NMR spectroscopy and the measurements of carbon detected ^1H spin relaxation times $T_1(^1H)$ and $T_{1\rho}(^1H)$ we were able to obtain detailed information on the primary structure, morphology and homogeneity of these materials down to the level of 0.5-100 nanometers. In this way, and particularly in reasonable experimental time, we were able to distinguish 4 distinct types of solid dispersions: (*i*) crystalline solid dispersions

containing nanocrystalline ASA in the crystalline PEG matrix; (*ii*) amorphous glass suspensions with large ASA crystallites embedded in amorphous pHPMA; (*iii*) solid solutions with molecularly dispersed ASA in amorphous PVP; and (*iv*) nano-heterogeneous solid solutions/suspensions containing nanosized ASA clusters dispersed in the matrix of PEOx (Figure 16). Our experimental findings revealed that the structural properties of these systems are determined by the combination of two factors: (*i*) accessibility and affinity of suitable molecular sites for the formation of hydrogen bonding between the API and the polymer matrix; and (*ii*) the segmental dynamics and T_g of the polymer coformers. (*For the details see papers D10 and D24 included to the dissertation*).

The received experiences were later implemented for investigating the structure properties of mucoadhesive buccal films (MBFs), which provide an innovative way to facilitate the efficient site-specific delivery of active compounds, while simultaneously separating the lesions from the environment of the oral cavity.[45] The problem we systematically investigated was the somewhat unintuitive behavior of MBFs of ciclopirox olamine (CPX) in a PEO matrix, where a dramatic decrease in CPX dissolution rates was observed for films with high CPX loadings.

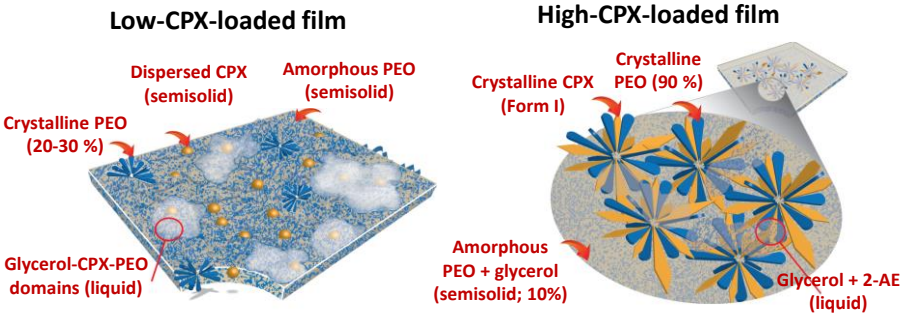

Figure 17. *Schematic representation of two distinct types of CPX/PEO mucoadhesive buccal films: the low-CPX-loaded film CPX0.2/PEO and the high-CPX system CPX1.8/PEO.*

Two distinct MBFs were identified: (*i*) at low CPX loading, a nanoheterogeneous solid solution of CPX molecularly dispersed in an amorphous PEO matrix was created; while (*ii*) at high CPX loading, a pseudo-co-crystalline system containing CPX−2-aminoethanol nanocrystals incorporated into the interlamellar space of a crystalline PEO matrix was formed (Figure 17). These structural differences were found to be closely related to the mechanical and physicochemical properties of the prepared MBFs. At low API loading, the polymer chains of PEO provided sufficient quantities of binding sites to stabilize the CPX that was molecularly dispersed in the highly amorphous semiflexible polymer matrix. Consequently, the resulting MBFs were soft, with low tensile strength, plasticity, and swelling index, supporting rapid drug release. At high CPX content, however, the active compounds and the polymer chains simultaneously co-crystallized, leaving the CPX to form nanocrystals grown directly inside the spherulites of PEO. Interfacial polymer−drug interactions were thus responsible not only for the considerably enhanced plasticity of the system, but also for the exclusive crystallization of CPX in the thermodynamically most stable polymorphic form, Form I, which exhibited reduced dissolution kinetics. (*For further details see paper D11 included to the dissertation*).

Thus, it is clear that the key factor in controlling the bioavailability and activity of drugs in solid formulations is the structure, arrangement and form of the active ingredient and its interaction with carriers and other excipients. However, these structural properties and the phenomena controlling the structural transformations are difficult to predict. Experimental knowledge is therefore still needed.

5.2. Active compounds in liquisolid drug delivery systems (D15)

Such a requirement is particularly challenging when active ingredients are formulated in forms that combine properties of liquid and solid phases. These *liquisolid* drug-delivery systems are basically powdered materials, which are based on incorporating the liquid films of a dissolved drug on the surface of mesoporous silica particles.[46] As a solvent typically the low-molecular weight PEO is used. Up to date a lot has been done in the synthesis of these systems, however, surprisingly little is known about the structure of the incorporated organic fraction; about the interface-affected internal architecture of the drug-solvent phase. Therefore, in a tight cooperation with the pharmaceutical companies TEVA Pharmaceuticals and Raciopharm, we investigated these systems with the aim to develop an easy-to-implement strategy allowing their reliable characterization even in industrial laboratories. This effort resulted in development of a surprisingly robust approach, which is based on a few straightforward ss-NMR techniques, which has no limitations regarding concentrations of the active compounds, and enables clear discrimination of various organic phases (Figure 18). Moreover, among a number of typical arrangements, a unique, previously unknown organogel phase of the self-assembled drug in a solvent was revealed. With an aid of 2D $^{1}H-^{1}H$ MAS NMR and quantum-chemical calculations this low molecular-weight organogel phase, existing in the porous system of the silica carrier, was described in detail (Figure 19). The optimized model revealed the tendency of API molecules to form hydrophobic arrangements through $-OH\cdots\pi$ interactions combined with $\pi-\pi$ stacking occurring in the core of API aggregates, preventing thus the formation of hydrogen bonds with the solvent. (*For the details see paper D15, which is included to the dissertation*).

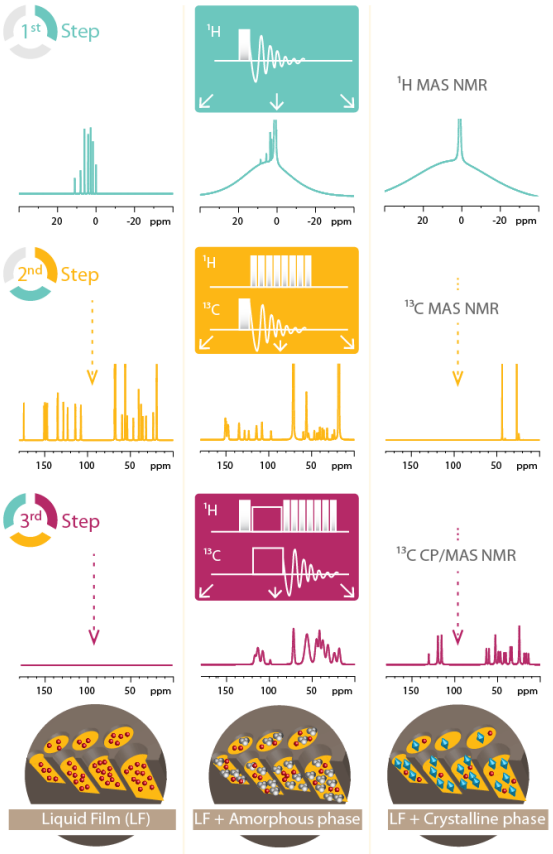

Figure 18. *Schematic representation of the three-step experimental strategy combining i) ^{1}H MAS NMR, ii) $T_1(^{13}C)$-filtered ^{13}C MAS NMR, and iii) ^{13}C CP/MAS NMR spectroscopy.*

Later we successfully applied this methodology to a number of other silica-based drug delivery systems.[47,48] The proposed approach, which allows to clearly discriminate a variety of local structures of active compounds loaded into mesoporous silica drug delivery devices in a reasonably short time, thus appears to be generally applicable to guide the advancement of novel drug delivery systems.

Overall, the discovery of a unique phase that exists exclusively in porous systems of carrier particles has accelerated the demand for the methods that allow the prediction and determination of molecular structures in complex multicomponent solids. And one of the best ways to do this has been modification of the NMR crystallography approach towards the domain-edited version.

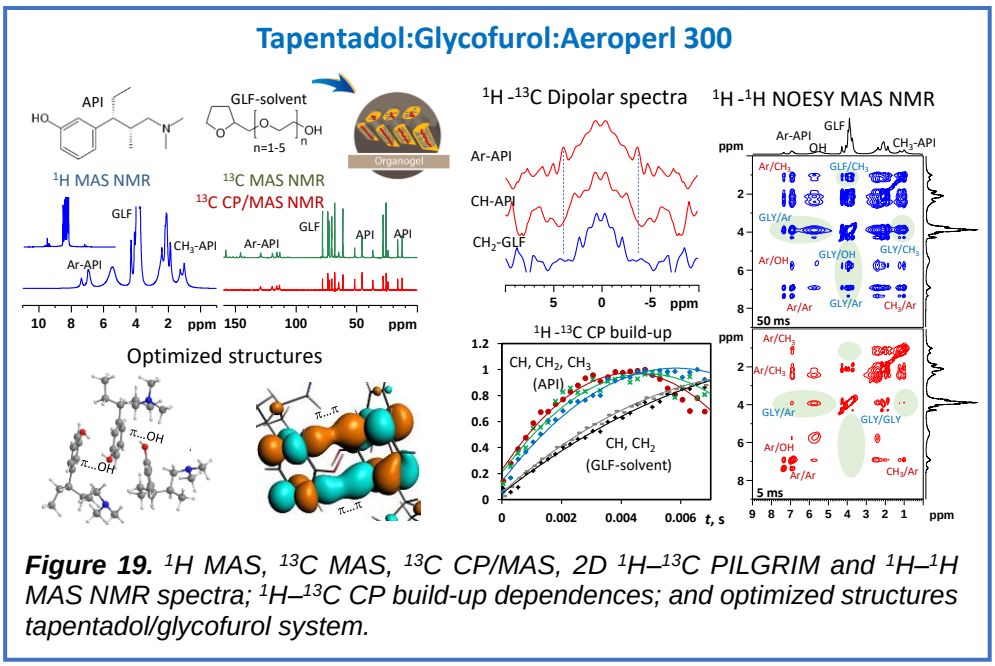

Figure 19. *¹H MAS, ¹³C MAS, ¹³C CP/MAS, 2D ¹H–¹³C PILGRIM and ¹H–¹H MAS NMR spectra; ¹H–¹³C CP build-up dependences; and optimized structures tapentadol/glycofurol system.*

5.3. Prediction of crystal structures and NMR crystallography (D25-D28)

NMR crystallography is a method that primarily uses ss-NMR spectroscopy, usually supplemented by quantum-chemical calculations and powder diffraction, to determine the structure of solid materials at the atomic scale. The main interest in NMR crystallography is in microcrystalline materials, which are amenable to this method but not to X-ray, neutron and electron diffraction. An original approach, which allows crystal structure determination solely from NMR data, is based on the analysis of ^{1}H-^{1}H spin diffusion combined with Monte Carlo simulations.[49] This approach, however; requires time-consuming measurements of a large set of high-resolution 2D ^{1}H-^{1}H correlation spectra.

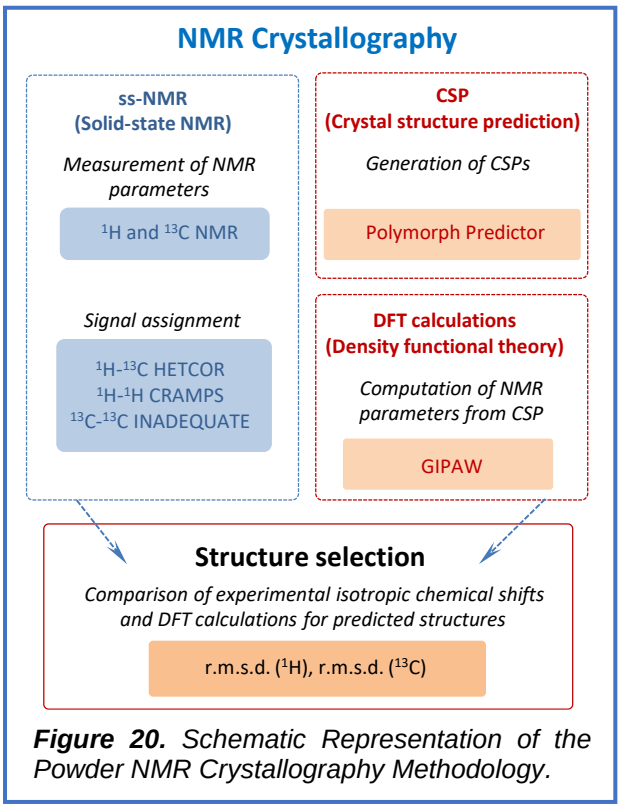

Figure 20. *Schematic Representation of the Powder NMR Crystallography Methodology.*

A much faster approach is based on the measurement of isotropic ^{1}H and ^{13}C chemical shifts and their systematic comparison with the theoretical values DFT calculated for model structures derived by a Crystal Structure Prediction (CSP) method (Figure 20).[50] In this regard, to explore the limitations of this approach, we focused on the previously unconsidered influence of long-range molecular packing on NMR parameters, when reconstructing the crystal structure of decitabine exclusively from ^{1}H and ^{13}C NMR chemical shifts. By calculating the NMR data, we found that symmetry operations significantly affected the molecular packing and unit cell parameters, while the conformations and short-range arrangements were virtually identical. Consequently, the NMR parameters of NMR-consistent models were similar and barely distinguishable by the standard deviations of the experimental and calculated ^{1}H and ^{13}C chemical shifts. Therefore, to refine the crystal structure selection, we simulated the entire 2D ^{1}H-^{13}C and ^{1}H-^{1}H DQ/SQ NMR correlation spectra (Figure 21). By determining the covariance, which is a quantitative measure

of the differences between the experimental and calculated 2D correlation signals, the set of NMR-consistent candidates was further narrowed down and the correct crystal structure was unambiguously identified. This way we confirmed that using an extended protocol involving analysis of 2D ss-NMR correlation spectra, NMR crystallography can be used to describe crystal structures differing in long-range molecular packing for which ss-NMR spectroscopy is otherwise less sensitive. (For the details see paper D25 included to the dissertation). The only prerequisite for using NMR crystallography and obtaining reliable results is the recording of high-resolution ss-NMR correlation spectra. Since 2004, however, we have been working to optimize the experimental techniques used to achieve this. (*For the details see paper D26*).

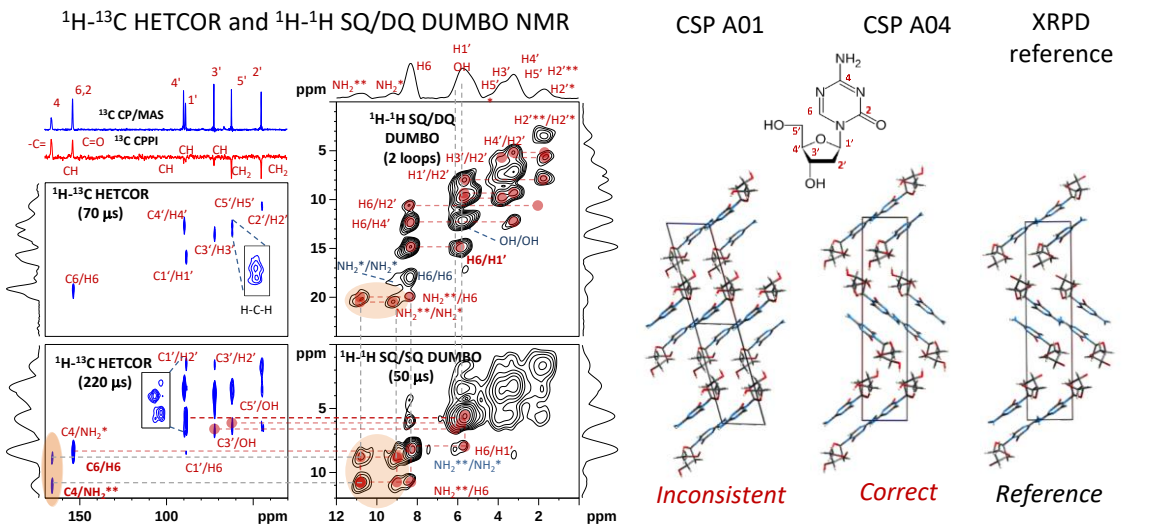

Figure 21. *Representative ss-NMR spectra of Decitabine and global molecular arrangements in CSPs A01 and A04 and the reference XRPD-refined crystal structure.*

Although the potentiality of this approach has been proven on several systems,[51] this methodology, has never been applied for the structure determination of really complex solids. The NMR crystallography is still rather applied in its simplified version, when ss-NMR is used to verify the XRPD-refined crystal structure. However, even this approach is limited, and the major limitation lies in the number of degrees of conformation freedom (DOF). Therefore, we developed a strategy, which allows to resolve structures with high DOF, while keeping the computational time reasonable. In this context, we treated the structure of the 32- and 38-DOF molecular systems, which belong among the most complex molecular structures ever solved *ab initio* from XRPD data. As the structure solution problem was on the edge of the current methodological possibilities, we applied a strategy using a combination of restraints from the Cambridge Structural Database, optimized simulated annealing parameters, and parallel code execution, all complemented by DFT-D calculations and analysis of ss-NMR parameters. (*For the details see papers D27 and D28 included to the dissertation*).

In summary, the whole concept of NMR crystallography is an integrated methodology that uses several techniques in combination to provide otherwise unavailable structural information, particularly for complex molecular solids for which direct crystal structure refinement using X-ray data does not give satisfactory results.

5.4. Domain-edited NMR crystallography (D29)

Polycrystalline composites with micro/nanodomain architecture, composed of a mixture of different crystalline and amorphous components, usually with a low amount of the key substance are then an example of the systems, where the atomic resolution structure remains a challenge, even in the presence of x-ray diffraction data. Typical representatives of these materials are drug delivery systems. For instance, due to the hydrolytic lability of decitabine (a

substance for leukemia treatment), injectable microbeads based on the micro-domains of the API incorporated in the semi-crystalline matrix of polysebacic acid were developed.[52] NMR crystallography was then an ideal base for obtaining the detailed structural information. The previously developed strategy, however; needed to be extended to generate structural data selectively for individual components. ss-NMR offers a range of techniques enabling selective manipulation with the signals. For polymeric composites, the T_1-relaxation filtered experiments are particularly suited. This is given by the fact, that local motions in even highly crystalline polymers reduce the ^{1}H spin−lattice relaxation times $T_1(^1H)$ to several seconds only, whereas the APIs usually exhibit $T_1(^1H)$ relaxation times reaching up to several hundreds of seconds.

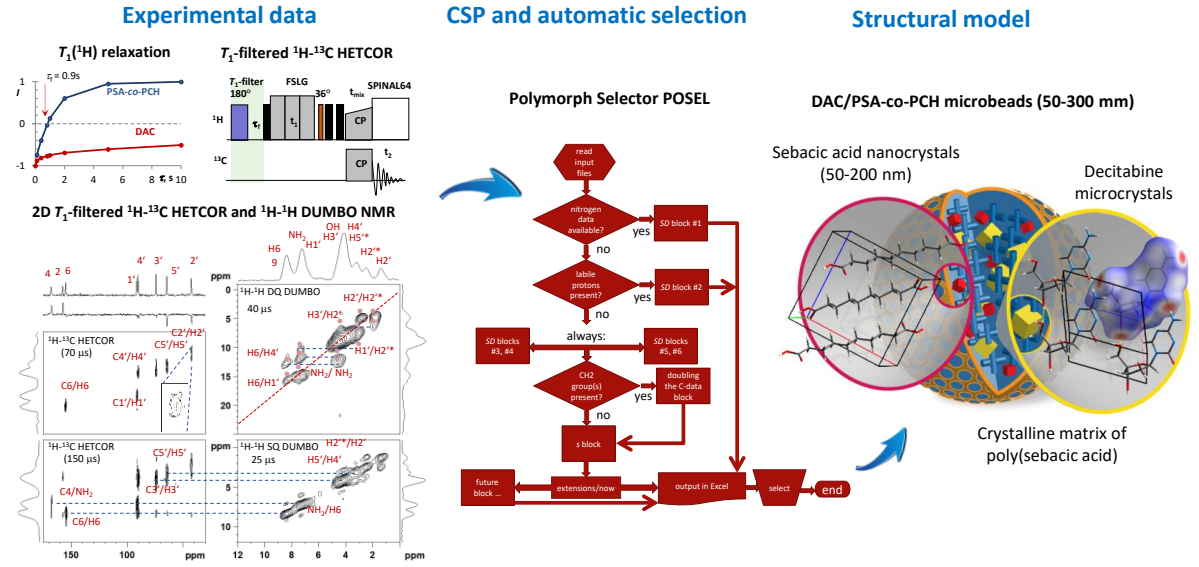

Figure 22. *$T_1(^1H)$ relaxation of decitabine and polymer matrix; T_1-filtered HETCOR pulse sequence; representative T_1-filtered ss-NMR spectra of microbead formulation of decitabine; schematic of automatic evaluation of predicted models and selected structures.*

Therefore, in order to consistently select individual components and thus to determine the corresponding isotropic chemical shifts precisely, we inserted the $T_1(^1H)$ relaxation filter into each NMR experiment (Figure 22). In the next step, the experimentally determined *domain-selective* NMR parameters were systematically compared with those calculated by DFT for the predicted crystal structures. This has been done using an automated protocol, POSEL-PolymorphSelector, developed by us (Figure 22, central panel). In this way, a group of CSPs was gradually narrowed down, and as a result of this search, the crystal structures of all the crystalline compounds dispersed in the polymer matrix were determined.

Overall, on the basis of differences in nuclear-spin relaxation the investigated microbeads were spectroscopically decomposed into the individual constituents revealing the presence of a crystalline polymeric matrix that is accompanied by the partly immobilized amorphous phase, microcrystallites of decitabine, and nanosized crystallites of sebacic acid. Using the proposed strategy an intricate structure of novel microbead formulations of decitabine was probed, and the atomic-resolution structure of the both types of dispersed crystallites was successfully determined (Figure 22, left panel). (*For the details see paper D29 included to the dissertation*).

The presented research demonstrates the synergy of combining several experimental and computational techniques, which extends the approach of NMR crystallography to the field of complex mixtures, nanostructured composites and even amorphous solids. Since the obtained results also open a way to structure refinement of synthetic polymers with a limited amount of available spectroscopic data, finding a procedure for reliable generation of a representative set of CSPs of synthetic polymers is of paramount importance.

6. Principle component analysis of ss-NMR spectra

The last part of the dissertation is devoted to the use of factor analysis of ss-NMR spectra for the structural characterization of amorphous fractions in multicomponent solids, thus opening up research towards understanding the structural regularities and diversity of the amorphous phase.

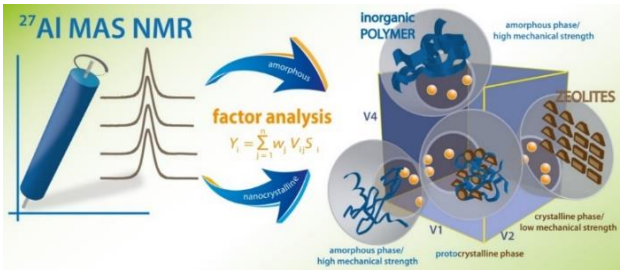

In current materials science, in an effort to develop advanced materials, amorphous alternatives of crystalline solids attract significant attention. For instance, in pharmaceutical industry, amorphous forms of active pharmaceutical ingredients belonging to BCS class II and IV have been shown to have favorable dissolution rates compared to the traditionally used crystalline formulations. Similarly, aluminosilicate inorganic polymers (geopolymers), the ceramic-like materials characterized by an amorphous three-dimensional Al-O-Si network have received considerable interest, because of their low cost, excellent mechanical properties, low energy consumption and reduced greenhouse emissions during manufacture. On the other hand, these amorphous materials are inherently unstable, and even small structural changes can result in significant variation in physicochemical properties.[53] Moreover, many of these amorphous solids exhibit certain degree of structural variability.[54] The origin of such variation, however; has not been fully explained, and the hypotheses involving the concept of rigid amorphous fraction (RAF), *pseudo-polyamorphism* or crystalline mesophase have been formulated.[54] Others, in this regard, rather consider the existence of more or less extensive *disorder* or *defects*, and a variety of concepts, including presence of a separated amorphous phase, molecular site disorder, and one-phase disorder, have been suggested. Each of these approaches has its own strong and weak points and supposes different physicochemical properties. The RAF is supposed to be associated with the nearly crystalline state (i.e. not showing T_g), whereas crystalline mesophase is more closely related to amorphous phase exhibiting T_g. From these presumptions is clear that the borderline between polymorphism, *polyamorphism* and the sample specific disorder is very thin.

It is thus obvious, that the advantages of amorphous modifications are subject to a heavy tax consisting in their difficult characterization. Due to inherent lack of periodic arrangement of building units and intrinsic motions, the explicit characterization of amorphous solids at the atomic level is very difficult and we are balancing on the physical and detection limits of traditionally used experimental techniques.

Inaccessible atomic-resolution structure of amorphous phase: In general, there is a wide range of methods suitable for characterization of crystalline solids: X-ray diffraction techniques, multinuclear ss-NMR and vibration spectroscopy are traditional tools. However, because of indistinct molecular arrangement in amorphous phase, the obtained spectroscopic and x-ray data are poorly resolved. Therefore, advanced techniques, such as pair-distribution function analysis of synchrotron powder diffraction data[55] or synchrotron-radiation-assisted infrared microscopy (SR-FTIR),[56] have been applied to obtain more detailed information. However, synchrotron-assisted techniques are not commonly accessible, and even the advanced 2D multiple-quantum MAS NMR techniques can fail because of rapid coherence decay.

Obviously, the amorphous phase generally does not provide high-resolution spectroscopic data, making it difficult to discern structural differences between different amorphous *phases* of a given compound. The conventionally obtained spectra are broadened and thus difficult to be interpreted by traditional approaches. Moreover, if the content of amorphous fractions is low; e.g. in the drug formulations, where the concentration of an amorphous drug is small, and strong signals of the filler compounds prevail; we are behind the detection limits of conventional analytical methods. In these cases, special procedures must be used.

6.1. Factor analysis of ^{19}F NMR spectra and polyamorphism (D30, D31)

In this regard we see a great potential in multivariate analysis of spectroscopic data, which is currently a routine procedure for the analysis of natural products, the spectra of which are crowded by a number of signals.[57] Analogously, the NMR spectra of amorphous and strongly disordered solids can be considered as an extreme limit, where the frequency range is so overcrowded by the signals of differently oriented molecules that only the envelope is detected. Consequently, the multivariate analysis of a set of these spectra can provide required discrimination of different amorphous products (forms) of a given compound. Following this idea, we focused on the application of *factor analysis* of low-resolution ss-NMR spectra for characterizing differently prepared amorphous forms of APIs in low-dose formulations.

Factor analysis (FA) using the singular value decomposition (SVD) algorithm allows the conversion of experimental NMR spectra Y_i into a set of subspectra S_j:

$$Y_i = \sum_{j=1}^{n} w_j V_{ij} S_j$$

The subspectra S_j are linear combinations of the experimental data and *vice versa*. Each subspectrum S_j represents a specific spectral feature that is typical for a given type of analyzed samples. The statistical importance of each subspectrum S_j is expressed by the singular value w_j. The ability of a particular subspectrum S_j to describe the experimental spectrum Y_i is expressed by the coefficient V_{ij}. The coefficients V_{ij} then represent quantitative parameters that reflect spectral differences between the analyzed samples. The structural differences between different amorphous forms thus can be in principle described by V_{ij} coefficients.

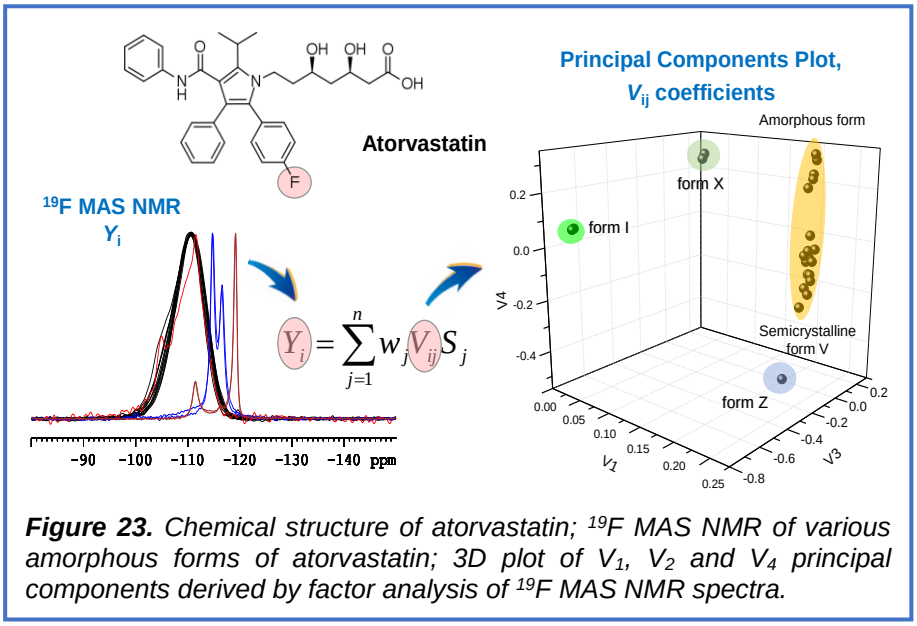

Figure 23. *Chemical structure of atorvastatin; ^{19}F MAS NMR of various amorphous forms of atorvastatin; 3D plot of V_1, V_2 and V_4 principal components derived by factor analysis of ^{19}F MAS NMR spectra.*

An example of the API which exhibits extreme structural variability is *atorvastatin*. Up to now more than 60 crystal forms of this compound have been claimed, and besides of 10 highly-crystalline forms a majority of these forms represents disordered and amorphous phases. Distinguishing of these amorphous forms, particularly in low-dose formulation when the strong signals of filler compounds dominate, is practically unattainable. Atorvastatin is, however, a compound containing fluorine atom; and this is great advantage. Due to the high gyromagnetic ratio and 100% isotopic abundance of fluorine atoms (^{19}F) the NMR receptivity for ^{19}F is 4700 times higher than that for ^{13}C. Moreover, almost none of excipients contain fluorine atoms. Therefore, ^{19}F NMR spectra can be acquired quickly even for diluted systems without the danger that ^{19}F NMR signals of the API are overlapped by the signals of excipients.

That is why, ^{19}F MAS NMR spectra of amorphous forms of atorvastatin are perfect example to demonstrate the application potential of factor analysis. The well-ordered crystalline forms (I and X) can be simply distinguished (Figure 23). On the other hand, differences between the

disordered and amorphous forms are very tiny, and apparently negligible (indistinct broadening at the left side of the spectra, Figure 23). However, by applying the factor analysis, the sample-specific coefficients $V_{ij}(^{19}F)$ characterizing every product were obtained. In a graphical representation these scores provide clear distinction of different amorphous forms (Figure 23, 3D plot). The applied method also offers the ability to identify and quantify various mixtures of different modifications. Predominantly, however; the proposed method allows fast characterization of low-dose products. By applying ^{19}F MAS NMR spectroscopy the acceptable spectra of tablet formulations containing ca 1-5% of the API can be recorded within 10-30 minutes, and thus the proposed method has the ability to reveal deviations from the expected output and identify undesired products of manufacture in real time. Moreover, nowadays approximately 20-25% of drugs in the pharmaceutical pipeline contain at least one fluorine atom. The potential use of this approach in the characterization of low-dose pharmaceutical formulations is therefore much broader.

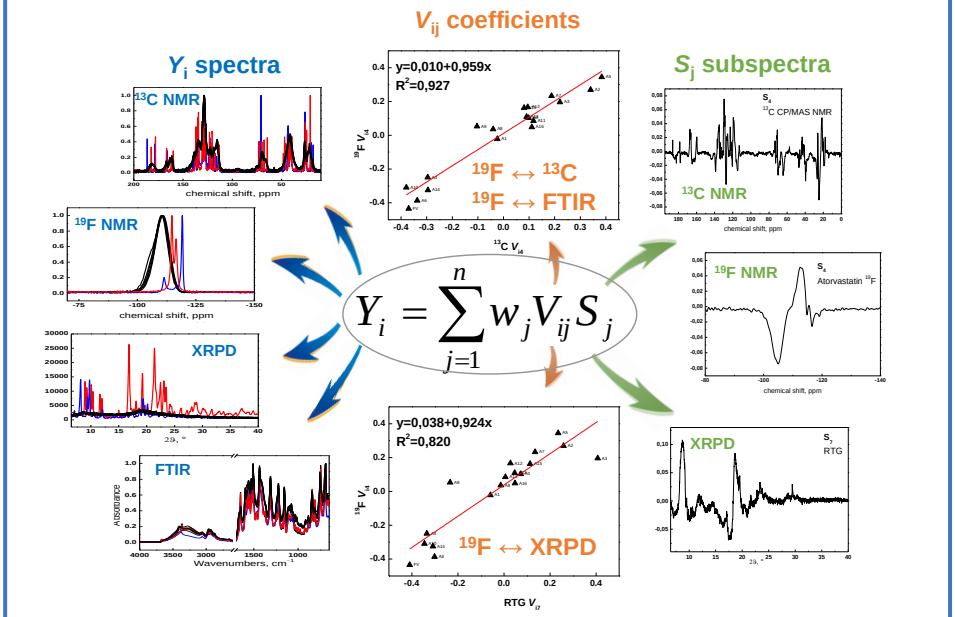

Figure 24. *^{19}F MAS NMR, ^{13}C CP/MAS NMR, FTIR and XRPD data of various amorphous forms of atorvastatin; linear regressions of $V_4(^{19}F)$;$V_4(^{13}C)$ and V_7(XRPD) components and the corresponding $S_4(^{19}F)$, $S_4(^{13}C)$, and S_7(XRPD) subspectra.*

In addition, when looking for the specific structural changes in amorphous phase we systematically compared V_{ij} scores obtained by the factor analysis of other spectroscopic results including ^{13}C CP/MAS NMR, FTIR and XRPD data (Figure 24, left side). Although the direct comparison of different types of spectroscopic data is very complicated, it is possible to do this by linear regression of V_{ij} coefficients. This way, we found clear correlations between the scores $V_4(^{19}F) \leftrightarrow V_4(^{13}C) \leftrightarrow V_5$(FTIR) $\leftrightarrow V_7$(XRPD) (Figure 24, central part). This finding thus confirms that the computed $V_4(^{19}F)$ scores can be considered as the structure-related parameters describing changes in molecular arrangement. Moreover, this fact also suggests that the corresponding subspectra reflect the most substantial spectroscopic changes induced by molecular *rearrangement* of the amorphous phase (Figure 24, right side). This way we thus identified the key structural units and motifs responsible for variability of the amorphous phase of atorvastatin. (*For the details see papers included to the dissertation D30 and D31*).

6.2. Nanocrystalline phases in amorphous geopolymers (D32)

Encouraged by the previous success we applied FA for the structural characterization of amorphous geopolymers containing protocrystalline phases, which are considered to be promising materials for sorption of pollutants. Specifically, to circumvent the complications

arising from the amorphous nature of aluminosilicate matrix and the low concentrations of the protocrystalline domains, we used factor analysis of ^{27}Al MAS NMR spectra. Although the ^{27}Al MAS NMR spectra were not able to visually provide clear differences between the analyzed systems, the factor analysis easily distinguished the fully amorphous materials from the geopolymers containing nanocrystalline phases (see Figure 25, left graph). The reliability of this procedure was verified by the factor analysis of ^{29}Si MAS NMR spectra, which provided the same clustering (Figure 25, right graph). Thus, factor analysis of relatively low-resolution ^{27}Al MAS NMR spectra has the ability to reveal the spectroscopic features corresponding to nanocrystalline phases. (*For the details see papers included to the dissertation D32*).

In summary, all the tests performed confirmed that the measurement of even low-resolution ss-NMR spectra in the combination with factor analysis offers a reliable tool for identifying structural differences in amorphous and strongly disordered systems. It was shown that even featureless ss-NMR spectra can be used to detect subtle differences between various products. Appropriately constructed graphical representations, i.e., 3D correlation plots of normalized V_{ij} parameters, clearly separated the investigated systems into the well-defined clusters, allowing the identification of materials containing traces of crystallites or protocrystalline phases that did not provide typical Bragg diffractions.

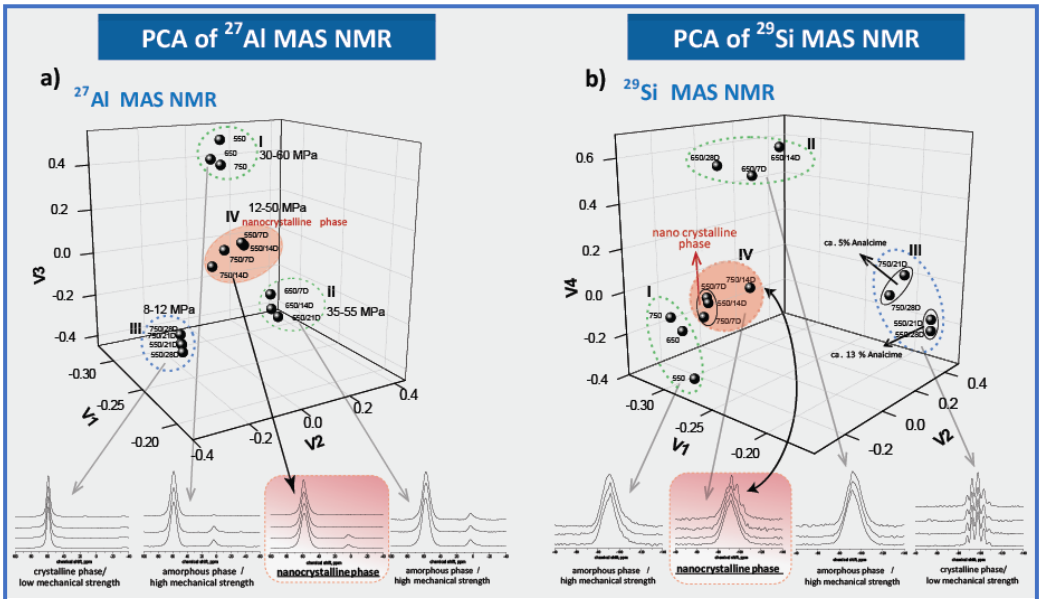

Figure 25. *^{27}Al MAS and ^{29}Si MAS NMR spectra of various geopolymers exhibited different crystallization tendencies; and the corresponding 3D plots of V_1, V_2 and V_4 principal components derived by the factor analysis of the recorded spectra.*

Overall, from the above-mentioned findings is clear, that factor analysis of spectroscopic data exhibits a potential to provide a new insight into the molecular organization of amorphous solids. Although the factor analysis cannot answer all of the questions related to the structural characterization of complex systems, the proposed strategy can help us to identify complex relationships that are often hidden under the surface of the first-order effects. In this regard, we performed further investigation of this approach and provided deeper insight into the uncommon polymorphism, or interfacial phenomena affecting mechanical properties of polymer microcomposites.[58]

7. Future perspectives

Solid-state NMR spectroscopy is a continuously developing branch of structural chemistry and is currently undergoing a phase of application of the recently developed experimental techniques to describe the structure of a new generation of functional materials. Further progress is expected in the area of structural characterization of amorphous phases, surfaces and interfaces. From an instrumental point of view, there is considerable potential in the field of dynamic nuclear polarization (DNP) and ultra-high field NMR spectroscopy (1.2 GHz and above). From a methodological point of view, machine learning and artificial intelligence will then become an integral part of the process of predicting and determining the structure of even extremely large and complex molecular systems.

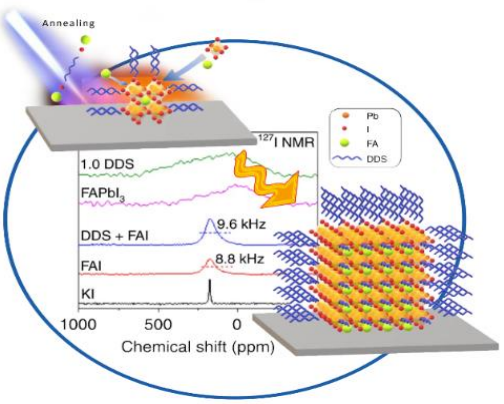

7.1. Machine learning as a tool to describe amorphous solids

In NMR spectroscopy there is a much more complex relationship between the resonance frequencies and molecular or crystal structure than there is in X-ray diffraction (XRD) spectroscopy between reflections and positions of atoms. In NMR spectroscopy, there is no analogy to Bragg law ($n\lambda = 2dsin\theta$) relating a diffraction angle θ, wavelength λ, and a separation distance *d* between atomic, or lattice, planes in the crystal. Thus, molecular modeling and high-level quantum-chemistry calculations need to be applied for an understanding of resonance frequencies in NMR spectra from the structural viewpoint. These calculations are, however, time-consuming and generally we are limited by a number of atoms present in the investigated molecular cluster. Importantly, for crystalline systems of the compounds featuring more than one-hundred atoms, the *periodic* density-functional theory (DFT) based calculations are clearly preferred to DFT computations that would apply *cluster* models. Nevertheless, the geometry optimization of a crystalline system can be exceedingly difficult even if the periodic DFT calculations are used. Specifically, we have recently demonstrated that it is possible to accurately describe the "propeller" polymorph of valinomycin ($C_{54}H_{90}N_6O_{18}$ that is a compound with 168 atoms), which has four molecules in the unit cell as big as about eight nm^3. However, due to a slow convergence of such optimization (250 optimization cycles were needed to meet the convergence criteria) and a big size of this solid-phase form (672 atoms in the unit cell), the computations took almost 18 days to finish on a high-performance server, where 60 cores of Intel® Xeon® Gold 6140@3.70 GHz processors were used. It should be noted, however, that an analogous DFT calculation for a cluster with 4*168 that is 672 atoms would be unfeasible,[59] although the most recent progress in this field is astonishing.[60]

Breakthroughs in this area are now being brought about by advanced NMR crystallography supported by the machine learning-based structure prediction, and by the use of artificial intelligence and large-scale NMR parameter calculations.[61] The machine learning approach developed by L. Emsley allows calculating of isotropic chemical shifts within seconds. Consequently, a representative set of model structures counting thousands of predictions can be processed in real time allowing thus cost-effective interpretation of NMR experimental data. In this way, the structures of several crystalline organics have already evaluated and verified with satisfactory agreement between theory and experiment. And even an attempt to predict

and determine structure of an amorphous through this large-state NMR predictions have been made.[62]

However, up to now only few papers utilizing this approach have been published and thus the wider application of the machine learning approach requires extensive verification, testing and calibration. Nevertheless, this approach promises to make key steps in resolving the problem of *polyamorphism*, when certain amorphous solids exhibit detectable structural variability. In particular, if the machine-learning large-scale NMR predictions will be combined with the factor analysis of the corresponding spectroscopic data, it would be possible to assign the NMR resonances extracted by the factor analysis to the structural motifs typical for a given amorphous phase in reasonable time (Figure 26). In general, we believe that it is precisely this concept that will make it possible to elucidate the structural regularities in amorphous solids in real time.

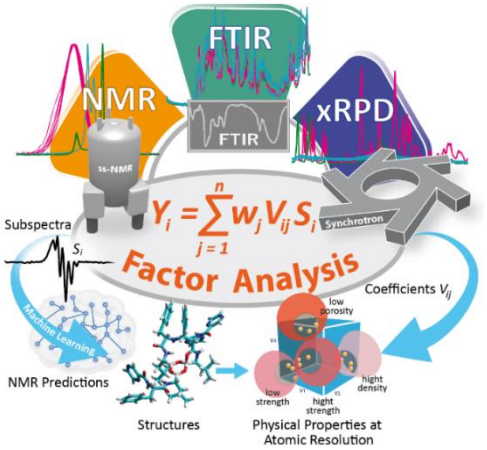

Figure 26. *Factor analysis for elucidating structural regularities in the amorphous phase of molecular solids.*

7.2. NMR crystallography of paramagnetic solids

Another field where one can expect great development is the structural analysis of energy-storage and energy-conversion materials, such as inorganic (metal halide perovskites), organic, and polymer solar cells offering a photovoltaic module with low production costs and relatively high efficiency. However, the accurate description of these usually *paramagnetic* systems is problematic. Specifically, in NMR spectroscopy the most challenging issue is the strong hyperfine interaction between the unpaired electrons and the observed nuclei. This interaction typically causes a large paramagnetic shift, extreme chemical shift anisotropy, and substantial enhancement of paramagnetic relaxation. These phenomena generally carry invaluable information about the bonding between atoms or ions, their spatial arrangement, delocalization of unpaired electrons towards the coordinating atoms and ligands, as well as allow explaining the corresponding optical properties. However, the presence of unpaired electrons causes serious problems in obtaining and interpreting the NMR spectra. The acquisition problem arises from extreme and difficult-to-predict paramagnetic shifts and chemical shift anisotropies, which are often so large that excitation of nuclear spins by commonly used radiofrequency powers is either ineffective or insufficiently broad, and/or both. Moreover, the large enhancement of paramagnetic relaxation induces an expressively fast decay of spin coherence, leading to a complete loss of the signal almost immediately after the excitation.

State-of-the-art experimental techniques of high-field ultra-wide-line NMR spectroscopy combined with modern computational quantum-chemistry approaches based on the relativistic density-functional theory (DFT) is, however; bringing clarity to this area. One of the simplest and surprisingly also most successful innovations lies in the application of Very-Fast Magic-Angle Spinning (VF/MAS) NMR technique (60-110 kHz), which enables the acquisition of highly resolved spectra without the need of any decoupling, or allows application of polarization transfer methods for characterization of even Mn(II) and Cu(II) containing compounds.[63] An important achievement allowing structural analysis of complex paramagnetic systems is based on the new *rf*-pulse schemes capable of broadband excitation such as short high-power adiabatic pulses (SHAP) combined with variable offset cumulative spectroscopy (VOCS) and

CPMG sequence.[64] Such pulse sequences enable a really broadband NMR response over a frequency range which is an order of magnitude larger than the applied *rf* field amplitude.[65]

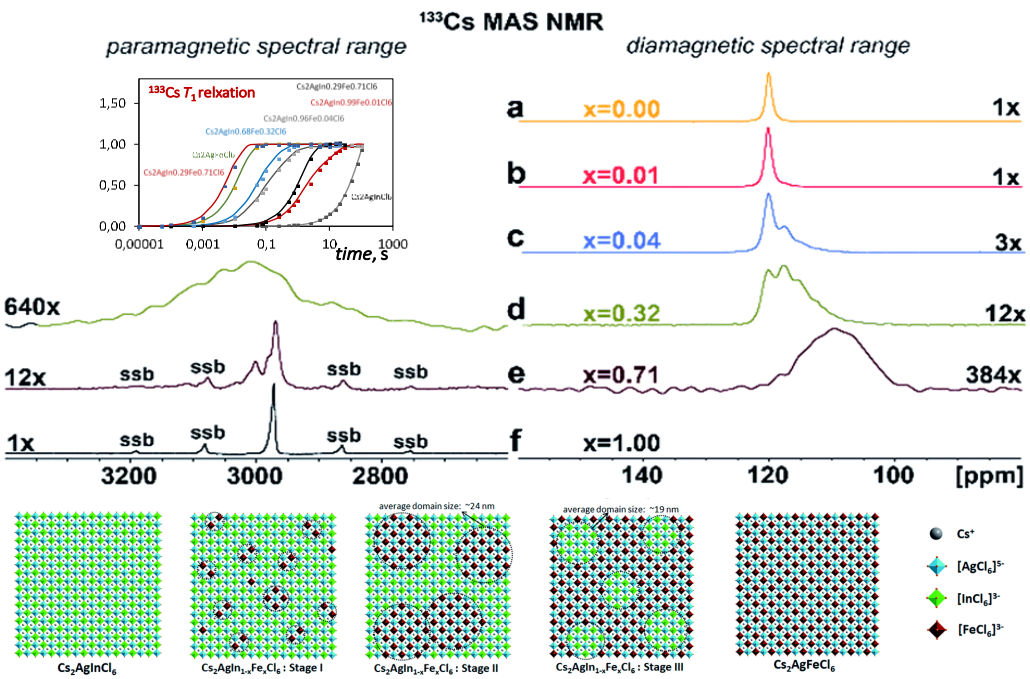

Figure 27. *Illustration of paramagnetic effects on ^{113}Cs NMR values of chemical shifts and spin-lattice relaxation times. The presence of paramagnetic alloying Fe^{3+} ions makes it possible to investigate the nuclear relaxation times, providing a straightforward approach to understand the distribution of paramagnetic species. The observed changes in ^{113}Cs NMR chemical shifts (3000 ppm) shows that paramagnetic Fe^{3+} replaces diamagnetic In^{3+} in the $Cs_2AgInCl_6$ lattice with the formation of $[FeCl_6]^{3-} \cdot [AgCl_6]^{5-}$ domains, which show different sizes and distribution modes in different alloying ratios.*

The structural investigation of paramagnetic solids thus presents a challenge that could not leave us calm. And so, since 2018, when we established a close collaboration with the *Department of Biomolecular and Organic Electronics at Linköping University*, we have begun extensively investigated the structure of materials with paramagnetic species.[66-70] For instance, in this research we described the atomic-level structure of bandgap engineered double perovskite alloys $Cs_2AgIn_{1-x}Fe_xCl_6$, when by analyzing the extreme paramagnetically induced NMR chemical shifts and spin relaxation times, we identified the domain structure of perovskite alloys (Figure 27).[66] For organic solar cells we have elucidated the role of intermolecular interactions in achieving high efficiency of novel organic solar cells,[69] or elucidated the role of Coulomb interactions in the formation of the molecular structure allowing to maximize the efficiency of unpaired electron transfer in the solar cell layer, in which the electron-hole (positive charge) transfer to the anode occurs.[70]

Despite these undeniable achievements, at high concentrations of paramagnetic particles, the local molecular structure in their immediate vicinity is difficult to access even using the above-mentioned techniques of ultra-wide-line NMR spectroscopy. Here we see two opportunities to look deeper into the structure of these materials at atomic resolution level. One possible way how to overcome this problem, and even to take advantage of the presence of unpaired electrons, is the application of dynamic nuclear polarization NMR (DNP-NMR).[71] This technique allows a large magnetic moment of unpaired electron spins to be transferred to nuclear spins during continuous microwave irradiation, thereby significantly increasing the

intensity of the corresponding NMR signals (Figure 28). Consequently, the signals of NMR active nuclei in vicinity of paramagnetic species are selectively several-fold amplified, which makes it possible to obtain the required structural information on the otherwise hidden matter.

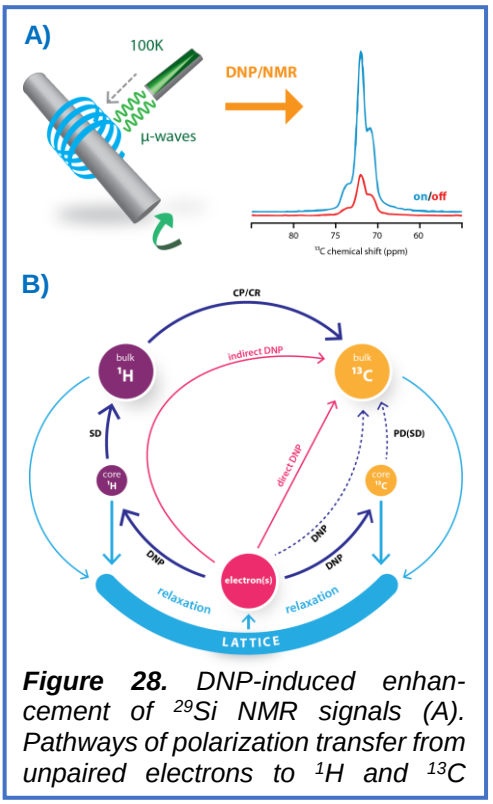

Figure 28. *DNP-induced enhancement of ^{29}Si NMR signals (A). Pathways of polarization transfer from unpaired electrons to ^{1}H and ^{13}C*

However, when going further, directly between the paramagnetic particles, inside to their clusters, to monitor their arrangement, architecture and mutual interactions, or to probe the transfer and reactions of radicals in hole transport layers of organic solar cells we will have to use alternative methods. In this regard I see the potential in a resonance method, which is known as *muon* spin resonance spectroscopy (μSR). Muons are particles with spin ½ that can be implanted into a wide range of solids and act as a local probe of the surrounding atomic environment. Measurement of the muon's precession and relaxation then provides an insight into the interactions with its local environment. This is given by the fact that muons have a very broad time window when measuring relaxation time, ranging from 10^{-4} to 10^{-11} s. This can thus provide unique information about the static and dynamic properties of the material of interest. As recently reported, μSR may be used to study energy storage materials, ionic diffusion in batteries, the dynamics of soft matter, free radical chemistry, reaction kinetics, semiconductors, advanced manufacturing and cultural artifacts.[72] But this is an entirely new story…

8. Conclusions

Over the last two decades, solid-state NMR spectroscopy has developed into a powerful and distinctive method of structural analysis, offering a variety of experimental techniques and approaches that allow the structure and dynamics of solids to be studied from different perspectives. My efforts, and those of my colleagues, have always been to describe the system under investigation as fully as possible, trying to understand the relationship between local segmental structure and dynamics, and macroscopic, physicochemical and end-use properties. The result of this systematic work is a set of experimental and computational methods optimized for specific types of organic, inorganic and hybrid solids. In some cases, through the synergistic interplay between measurements, calculations and statistical analysis, we have developed integrated strategies that provided otherwise unavailable structural information for complex multi-component systems in different physical states (liquids, solids, gels). The applied combinations of experimental and theoretical approaches then enabled one to determine the structural arrangements of molecules in situations that were not amenable to conventional spectroscopic techniques. Although there does not seem to be a universal and guaranteed way to look easily and always in real time into the heart of matter (of solid matter, of course), I am convinced that solid-state NMR spectroscopy offers at least one path to follow.

9. Publications that form the basis of the dissertation

D1 J. Brus*, J. Dybal, P. Schmidt, J. Kratochvíl, and J. Baldrian, **Order and Mobility in Polycarbonate−Poly(ethylene oxide) Blends Studied by Solid-State NMR and Other Techniques**
Macromolecules **2000** *33* (17), 6448-6459
IF=6.057; citations 52; Q1; JIF percentile 89.44 (in 2021).

D2 J. Brus*, J. Dybal, P. Sysel, and R. Hobzová, **Mobility, Structure, and Domain Size in Polyimide−Poly(dimethylsiloxane) Networks Studied by Solid-State NMR Spectroscopy**
Macromolecules **2002** *35* (4), 1253-1261
IF=6.057; citations 29; Q1; JIF percentile 89.44 (in 2021).

D3 Jiri Brus* and Jiří Dybal, **Hydrogen-Bond Interactions in Organically-Modified Polysiloxane Networks Studied by 1D and 2D CRAMPS and Double-Quantum ^{1}H MAS NMR**
Macromolecules **2002** *35* (27), 10038-10047
IF=6.057; citations 43; Q1; JIF percentile 89.44 (in 2021).

D4 Jiri Brus*, Milena Špírková, Drahomíra Hlavatá, and Adam Strachota, **Self-Organization, Structure, Dynamic Properties, and Surface Morphology of Silica/Epoxy Films as Seen by Solid-State NMR, SAXS, and AFM,** *Macromolecules* **2004** *37* (4), 1346-1357
IF=6.057; citations 84; Q1; JIF percentile 89.44 (in 2021).

D5 J Brus*, M Urbanova, J Czernek, M Pavelkova, K Kubova, J Vyslouzil, S Abbrent, R Konefal, J Horský, D Vetchy, J Vysloužil, P Kulich, **Structure and Dynamics of Alginate Gels Cross-Linked by Polyvalent Ions Probed via Solid-State NMR Spectroscopy** *Biomacromolecules* **2017** *18* (8), 2478-2488
IF=6.978; citations 99; Q1; JIF percentile 80.57 (in 2021).

D6 M Urbanova, M Pavelkova, J Czernek, K Kubova, J Vyslouzil, A Pechova, D Molinkova, J Vyslouzil, D Vetchy, J Brus* **Interaction Pathways and Structure–Chemical Transformations of Alginate Gels in Physiological Environments,** *Biomacromolecules* **2019** *20* (11), 4158-4170
IF=6.978; citations 29; Q1; JIF percentile 80.57 (in 2021).

D7 J Brus*, M Urbanová, and A Strachota **Epoxy Networks Reinforced with Polyhedral Oligomeric Silsesquioxanes: Structure and Segmental Dynamics as Studied by Solid-State NMR**
Macromolecules **2008** *41* (2), 372-386, DOI: 10.1021/ma702140g
IF=6.057; citations 89; Q1; JIF percentile 89.44 (in 2021).

D8 P Matějíček, J Brus, A Jigounov, J Pleštil, M Uchman, K Procházka, M Gradzielski **On the Structure of Polymeric Composite of Metallacarborane with Poly(ethylene oxide),**
Macromolecules **2011** *44* (10), 3847-3855, DOI: 10.1021/ma200502t
IF=6.057; citations 38; Q1; JIF percentile 89.44 (in 2021).

D9 J Brus*, A Zhigunov, J Czernek, L Kobera, M Uchman, P Matějíček **Control over the Self-Assembly and Dynamics of Metallacarborane Nanorotors by the Nature of the Polymer Matrix: A Solid-State NMR Study** *Macromolecules* **2014** *47* (18), 6343-6354, DOI: 10.1021/ma501117a
IF=6.057; citations 32; Q1; JIF percentile 89.44 (in 2021).

D10 Olivia Policianova, Jiri Brus*, Martin Hruby, Martina Urbanova, Alexander Zhigunov, Jana Kredatusova, and Libor Kobera **Structural Diversity of Solid Dispersions of Acetylsalicylic Acid as Seen by Solid-State NMR,** *Molecular Pharmaceutics* **2014** *11* (2), 516-530, DOI: 10.1021/mp400495h
IF=5.364; citations 54; Q1; JIF percentile 76.88 (in 2021).

D11 Martina Urbanova, Marketa Gajdosova, Miloš Steinhart, David Vetchy, and Jiri Brus* **Molecular-Level Control of Ciclopirox Olamine Release from Poly(ethylene oxide)-Based Mucoadhesive Buccal Films: Exploration of Structure–Property Relationships with Solid-State NMR**
Molecular Pharmaceutics **2016** *13* (5), 1551-1563, DOI: 10.1021/acs.molpharmaceut.6b00035
IF=5.364; citations 15; Q1; JIF percentile 76.88 (in 2021).

D12 Jiri Brus*and Martina Urbanova **Selective Measurement of Heteronuclear ^{1}H–^{13}C Dipolar Couplings in Motionally Heterogeneous Semicrystalline Polymer Systems**
The Journal of Physical Chemistry A **2005** *109* (23), 5050-5054, DOI: 10.1021/jp0503821
IF=2.944; citations 23; Q3; JIF percentile 37.73 (in 2021).

D13 Jiri Brus*, Martina Urbanová, Ivan Kelnar, and Jiří Kotek **A Solid-State NMR Study of Structure and Segmental Dynamics of Semicrystalline Elastomer-Toughened Nanocomposites**
Macromolecules **2006** *39* (16), 5400-5409, DOI: 10.1021/ma0604946
IF=6.057; citations 45; Q1; JIF percentile 89.44 (in 2021).

D14 Jiri Brus*, Jiri Czernek, Martina Urbanova, Jan Rohlíček, and Tomáš Plecháček
Transferring Lithium Ions in the Nanochannels of Flexible Metal–Organic Frameworks Featuring

	Superchaotropic Metallacarborane Guests: Mechanism of Ionic Conductivity at Atomic Resolution *ACS Applied Materials & Interfaces* **2020** *12* (42), 47447-47456, DOI: 10.1021/acsami.0c12293 *IF=10.383; citations 18; Q1; JIF percentile 85.94 (in 2021).*
D15	J Brus*, W Albrecht, F Lehmann, J Geier, J Czernek, M Urbanova, L Kobera, A Jegorov **Exploring the Molecular-Level Architecture of the Active Compounds in Liquisolid Drug Delivery Systems Based on Mesoporous Silica Particles: Old Tricks for New Challenges** *Molecular Pharmaceutics* **2017** *14* (6), 2070-2078, DOI: 10.1021/acs.molpharmaceut.7b00167 *IF=5.364; citations 21; Q1; JIF percentile 76.88 (in 2021).*
D16	L Kobera, J Czernek, M Strečková, M Urbanova, S Abbrent, J Brus* **Structure and Distribution of Cross-Links in Boron-Modified Phenol–Formaldehyde Resins Designed for Soft Magnetic Composites: A Multiple-Quantum ^{11}B–^{11}B MAS NMR Correlation Spectroscopy Study** *Macromolecules* **2015** *48* (14), 4874-4881, DOI: 10.1021/acs.macromol.5b01037 *IF=6.057; citations 24; Q1; JIF percentile 89.44 (in 2021).*
D17	J. Brus*, J. Czernek, M. Urbanova, L. Kobera and A. Jegorov, **An efficient 2D ^{11}B–^{11}B solid-state NMR spectroscopy strategy for monitoring covalent self-assembly of boronic acid-derived compounds: the transformation and unique architecture of bortezomib molecules in the solid state,** *Phys. Chem. Chem. Phys.,* **2017,***19***,** 487-495, DOI: 10.1039/C6CP06555D *IF=3.945; citations 20; Q2; JIF percentile 51.23 (in 2021).*
D18	C Xu, G Hernández, S Abbrent, L Kobera, R Konefal, J Brus, K Edström, D Brandell, J Mindemark **Unraveling and Mitigating the Storage Instability of Fluoroethylene Carbonate-Containing LiPF6 Electrolytes To Stabilize Lithium Metal Anodes for High-Temperature Rechargeable Batteries** *ACS Applied Energy Materials* **2019** *2* (7), 4925-4935, DOI: 10.1021/acsaem.9b00607 *IF=6.959; citations 37; Q2; JIF percentile 73.31 (in 2021).*
D19	J Li, R Fernandez-Alvarez, Z Tošner, P Kozlík, M Štěpánek, A Zhigunov, M Urbanová, J Brus, M Uchman, P Matějíček **Polynorbornene-Based Polyelectrolytes with Covalently Attached Metallacarboranes: Synthesis, Characterization, and Lithium-Ion Mobility**, *Macromolecules* **2021** 54 (14), 6867-6877, DOI: 10.1021/acs.macromol.1c00350 *IF=6.057; citations 4; Q1; JIF percentile 89.44 (in 2021).*
D20	FP Nkosi, M Valvo, J Mindemark, NA Dzulkurnain, G Hernández, A Mahun, S Abbrent, J Brus, L Kobera, K Edström **Garnet-Poly(ε-caprolactone-co-trimethylene carbonate) Polymer-in-Ceramic Composite Electrolyte for All-Solid-State Lithium-Ion Batteries**, *ACS Applied Energy Materials* **2021** *4* (3), 2531-2542, DOI: 10.1021/acsaem.0c03098 *IF=6.959; citations 23; Q2; JIF percentile 73.31 (in 2021).*
D21	J Brus*, L Kobera, M Urbanová, D Koloušek, J Kotek, **Insights into the Structural Transformations of Aluminosilicate Inorganic Polymers: A Comprehensive Solid-State NMR Study** *J Phys Chem C* **2012** *116* (27), 14627-14637, DOI: 10.1021/jp300181q *IF=4.177; citations 32; Q2; JIF percentile 53.07 (in 2021).*
D22	J Brus*, L Kobera, M Urbanova, B Doušová, M Lhotka, D Koloušek, J Kotek, P Čuba, J Czernek, J Dědeček **Interface Induced Growth and Transformation of Polymer-Conjugated Proto-Crystalline Phases in Aluminosilicate Hybrids: A Multiple-Quantum ^{23}Na–^{23}Na MAS NMR Correlation Spectroscopy Study.** *Langmuir* **2016** *32* (11), 2787-2797, DOI: 10.1021/acs.langmuir.5b04736 *IF=4.331; citations 13; Q2; JIF percentile 60.06 (in 2021).*
D23	J Brus, L Kobera, W Schoefberger, M Urbanová, P Klein, P Sazama, E Tabor, S Sklenak, AV Fishchuk, J Dědeček **Structure of Framework Aluminum Lewis Sites and Perturbed Aluminum Atoms in Zeolites as Determined by ^{27}Al{^{1}H} REDOR (3Q) MAS NMR Spectroscopy and DFT/Molecular Mechanics,** *Angew Chem – Int. Edition* **2015,** 54 (2), 541, https://doi.org/10.1002/anie.201409635 *IF=16.823; citations 77; Q1; JIF percentile 91.90 (in 2021).*
D24	Urbanova, M., Sturcova, A., Kredatusova, J., Brus J.* **Structural insight into the physical stability of amorphous Simvastatin dispersed in pHPMA: Enhanced dynamics and local clustering as evidenced by solid-state NMR and Raman spectroscopy** *Int.l J Pharm* **2015**, 478(2), pp. 464-475, https://doi.org/10.1016/j.ijpharm.2014.12.007 *IF=6.510; citations 9; Q1; JIF percentile 85.84 (in 2021).*
D25	Jiri Brus*, Jiri Czernek, Libor Kobera, Martina Urbanova, Sabina Abbrent, and Michal Husak **Predicting the Crystal Structure of Decitabine by Powder NMR Crystallography: Influence of Long-Range Molecular Packing Symmetry on NMR Parameters** *Crystal Growth & Design* **2016** *16* (12), 7102-7111, DOI: 10.1021/acs.cgd.6b01341 *IF=4.010; citations 19; Q1; JIF percentile 82.69 (in 2021).*

D26	Jiri Brus*and Alexandr Jegorov **Through-Bonds and Through-Space Solid-State NMR Correlations at Natural Isotopic Abundance: Signal Assignment and Structural Study of Simvastatin** *The Journal of Physical Chemistry A* **2004** *108* (18), 3955-3964, DOI: 10.1021/jp0498163 *IF=2.944; citations 53; Q3; JIF percentile 37.73 (in 2021).*
D27	Michal Hušák, Alexandr Jegorov, Jan Rohlíček, Andrew Fitch, Jiří Czernek, Libor Kobera, and Jiri Brus* **Determining the Crystal Structures of Peptide Analogs of Boronic Acid in the Absence of Single Crystals: Intricate Motifs of Ixazomib Citrate Revealed by XRPD Guided by ss-NMR** *Crystal Growth & Design* **2018** *18* (6), 3616-3625, DOI: 10.1021/acs.cgd.8b00402 *IF=4.010; citations 21; Q1; JIF percentile 82.69 (in 2021).*
D28	M Hušák, A Jegorov, J Czernek, J Rohlíček, S Žižková, P Vraspír, P Kolesa, A Fitch, J Brus* **Successful Strategy for High Degree of Freedom Crystal Structure Determination from Powder X-Ray Diffraction Data: A Case Study for Selexipag Form I with 38 DOF** *Crystal Growth & Design* **2019** 19 (8), 4625-463, DOI: 10.1021/acs.cgd.9b00517 *IF=4.010; citations 11; Q1; JIF percentile 82.69 (in 2021).*
D29	Jiri Brus*, Jiri Czernek, Martin Hruby, Pavel Svec, Libor Kobera, Sabina Abbrent, and Martina Urbanova **Efficient Strategy for Determining the Atomic-Resolution Structure of Micro- and Nanocrystalline Solids within Polymeric Microbeads: Domain-Edited NMR Crystallography** *Macromolecules* **2018** *51* (14), 5364-5374, DOI: 10.1021/acs.macromol.8b00392 *IF=6.057; citations 15; Q1; JIF percentile 89.44 (in 2021).*
D30	Jiri Brus*, Martina Urbanova, Ivana Sedenkova, Hana Brusova **New perspectives of ^{19}F MAS NMR in the characterization of amorphous forms of atorvastatin in dosage formulations** *Int J Pharm* **2011** 409(1-2), pp. 62-74, https://doi.org/10.1016/j.ijpharm.2011.02.030 *IF=6.510; citations 50; Q1; JIF percentile 85.84 (in 2021).*
D31	Urbanová M., Brus J.*, Šeděnková I., Policianová O., Kobera L. **Characterization of solid polymer dispersions of active pharmaceutical ingredients by ^{19}F MAS NMR and factor analysis** *Spectrochimica Acta Part A-Molecular and Biomolecular Spectroscopy* **2013**, 100, 59-66. https://doi.org/10.1016/j.saa.2012.02.057 *IF=4.831; citations 27; Q1; JIF percentile 89.53 (in 2021).*
D32	Urbanová M., Kobera L., Brus J.* **Factor analysis of ^{27}Al MAS NMR spectra for identifying nanocrystalline phases in amorphous geopolymers** *Magnetic Resonance in Chemistry*. 51/11 (**2013**), 734-742, https://doi.org/10.1002/mrc.4009 *IF=2.392; citations 17; Q3; JIF percentile 36.03 (in 2021).*

10. References *(Author's publications are indicated in red)*

1) Lowe, I.J. Free Induction Decays of Rotating Solids, *Phys. Rev. Lett.*, **1959**, *2*, 285.
2) Langer, B.; Schnell, I.; Spiess, H.W.; Grimmer, A.R. Temperature calibration under ultrafast MAS conditions. *J. Magn. Reson.* **1999**, *138*, 182-186.
3) Brus, J. Heating of Samples Induced by Fast Magic-Angle Spinning. *Solid State Nucl. Magn. Reson*. **2000**, *16*, 151-160.
4) Waugh, J.S.; Huber, L.M.; Haeberlen, U. Approach to High-Resolution nmr in Solids, *Phys. Rev. Lett.,* **1968**, *20*, 180.
5) Maciel, G.E.; Bronnimann, C.E.; Hawkins, B. High-resolution 1H nmr in solids via CRAMPS, *Adv. Magn. Reson.* **1990**, *14*, 125.
6) van Rossum, B.-J.; Förster, H.; de Groot, H.J.M. High-field and high-speed CP-MAS13C NMR heteronuclear dipo-lar-correlation spectroscopy of solids with frequency-switched Lee–Goldburg homonuclear decoupling. *J. Magn. Reson.* **1997**, *124*, 516-519.
7) D. Sakellariou, A. Lesage, P. Hodgkinson, L. Emsley, Homonuclear dipolar decoupling in solid-state NMR using continuous phase modulation, *Chem. Phys. Lett.*, **2000**, 319, 253.
8) Moutzouri, P.; Simões de Almeida, B.; Torodii, D.; Emsley, L. Pure Isotropic Proton Solid State NMR, *J. Am. Chem. Soc.* **2021**, *143*, 26, 9834.
9) Moutzouri, P., Cordova, M., Simões de Almeida, B., Torodii, D., Emsley, L., Two-dimensional Pure Isotropic Proton Solid State NMR, *Angew. Chem. Int. Ed.* 2023, 62, e202301963; *Angew. Chem.* **2023**, *135*, e202301963.
10) Bloembergen, N. On the interaction of nuclear spins in a crystalline lattice, *Physica* **1949**, *15*, 386.
11) Demco, D.E.; Johanson, A.; Tegenfeldt, J. Proton spin diffusion for spatial heterogeneity and morphology investigations of polymers, *Solid State Nucl Magn Reson* **1995**, *4*, 13.
12) VanderHart, D.L.; McFadden, G.B. Some perspectives on the interpretation of proton NMR spin diffusion data in terms of polymer morphologies, *Solid State Nucl Magn Reson* **1996**, *7*, 45.
13) Schmidt-Rohr K.; Clauss J.; Spiess H.W. Correlation of Structure and Mobility and Morphology by 2D Wideline-

Separation NMR, *Macromolecules* **1992**, *25*, 3273.
14) Mellinger, F.; Wilhelm, M.; Spiess, H.W. Calibration of ^{1}H NMR Spin Diffusion Coefficients for Mobile Polymers through Transverse Relaxation Measurements, *Macromolecules* **1999**, *32*, 4686.
15) Yan, B.; Stark, R.E. A WISE NMR Approach to Heterogeneous Biopolymer Mixtures: Dynamics and Domains in Wounded Potato Tissues, *Macromolecules* **1998**, *31*, 2600.
16) Palmer, A.G.; Williams, J.; McDermott, A. Nuclear Magnetic Resonance Studies of Biopolymer Dynamics, *J. Phys. Chem.* **1996**, *100*, 13293.
17) Huster, D.; Xiao, L.S.; Hong, M. Solid-state NMR investigation of the dynamics of the soluble and membrane-bound colicin Ia channel-forming domain, *Biochemistry* **2001**, *40*, 7662.
18) Lipari, G.; Szabo, A. Model-free approach to the interpretation of nuclear magnetic resonance relaxation in macromolecules. 1. Theory and range of validity, *J. Am. Chem. Soc.* **1982**, *104*, 4546.
19) Hong, M.; Yao, X.L.; Jakes, K.; Huster, D. Investigation of molecular motions by Lee-Goldburg cross-polarization NMR Spectroscopy. *J. Phys. Chem. B* **2002**, *106*, 7355.
20) Ramamoorthy, A.; Wei, Y.F.; Lee, D.K. PISEMA solid-state NMR spectroscopy. *Annual Reports on NMR Spectroscopy* **2004**, *52*, 1-52.
21) Kay, E. R.; Leigh, D. A.; Zerbetto, F. Synthetic molecular motors and mechanical machines, *Angew. Chem., Int. Ed.* **2007**, *46*, 72-191.
22) Dominguez, Z.; Dang, H.; Strouse, M. J.; Garcia-Garibay, M. A. Molecular “compasses” and “gyroscopes.” III. Dynamics of a phenylene rotor and clathrated benzene in a slipping-gear crystal lattice, *J. Am. Chem. Soc.* **2002**, *124*, 7719.
23) Hawthorne, M. F.; Zink, J. I.; Skeleton, J. M.; Bayer, M. J.; Liu, C.; Livshits, E.; Baer, R.; Neuhauser, D. Electrical or photocontrol of the rotary motion of a metallacarborane, *Science* **2004**, *303*, 1849.
24) Xue, M.; Wang, K. L., Molecular Rotors as Switches. *Sensors* **2012**, *12*, 11612.
25) Karlen, S. D.; Reyes, H.; Taylor, R. E.; Khan, S. I.; Hawthorne, M. F.; Garcia-Garibay, M. A. Symmetry and dynamics of molecular rotors in amphidynamic molecular crystals, *PNAS* **2010**, *107*, 14973.
26) Brus, J.; Czernek, J.; Urbanova, M.; Červinka, C. Enantiotropy of Simvastatin as a Result of Weakened Interactions in the Crystal Lattice: Entropy-Driven Double Transitions and the Transient Modulated Phase as Seen by Solid-State NMR Spectroscopy. *Molecules* **2022**, *27*, 679.
27) Wu, Y.; Sun, B. Q.; Pines, A.; Samoson, A.; Lippmaa, E. NMR Experiments with a New Double Rotor, *J. Magn. Reson.* **1990**, *89*, 297.
28) Eastman, M. A.; Grandinetti, P. J.; Lee, Y.K.; Pines, A. Double-Tuned Hopping-Coil Probe for Dynamic-Angle-Spinning NMR, *J. Magn. Reson.* **1992**, *98*, 333-341.
29) Samoson, A.; Lippmaa, E.; Pines, A. High-Resolution Solid-State NMR Averaging of 2nd-Order Effects by Means of a Double-Rotor, *Mol. Phys.* **1988**, *65*, 1013-1018.
30) Chmelka, B. F.; Mueller, K.T.; Pines, A.; Stebbins, J.; Wu, Y.; Zwanziger, J. W. O-17 NMR in Solids by Dynamic-Angle Spinning and Double Rotation, *Nature* **1989**, *339*, 42-43.
31) Medek, A.; Harwood, J. S.; Frydman, L. Multiple-Quantum Magic-Angle Spinning NMR: A New Method for the Study of Quadrupolar Nuclei in Solids, *J. Am. Chem. Soc.*, **1995**, 117, 12779-12787.
32) Amoureux, J. P.; Fernandez, C.; Steuernagel, S. Z Filtering in MQMAS NMR, *J. Magn. Reson., Ser. A* **1996**, *123*, 116-118.
33) Brus, J.; Abbrent, S.; Kobera, L.; Urbanova, M.; Cuba, P. Advances in 27Al MAS NMR Studies of Geopolymers, *Annual Reports on NMR Spectroscopy* **2016**, *88*, 79-147.
34) Kobera, L.; Brus, J.; Klein, P.; Dedecek, J.; Urbanova M. Biaxial Q-shearing of 27Al 3QMAS NMR spectra: Insight into the structural disorder of framework aluminosilicates, *Solid State Nucl. Magn. Reson*. **2014**, *57*, 29.
35) Ashbrook, S. E.; Wimperis, S. Satellite-Transition MAS NMR of Spin I=3/2, 5/2, 7/2, and 9/2 Nuclei: Sensitivity, Resolution, and Practical Implementation, *J. Magn. Reson.*, **2002**, *156*, 269-281.
36) Amoureux, J. P.; Morais, C.; Trebosc, J.; Rocha, J.; Fernandez, C. I-STMAS, a New High-Resolution Solid-State NMR Method for Half-Integer Quadrupolar Nuclei, *Solid State Nucl. Magn. Reson.* **2003**, *23*, 213-223.
37) Yao, Z.; Kwak, H.T.; Sakellariou, D.; Emsley, L.; Grandinetti, P. J. Sensitivity Enhancement of the Central Transition NMR Signal of Quadrupolar Nuclei under Magic-Angle Spinning. *Chem. Phys. Lett.*, **2000**, *327*, 85.
38) Wang, Q.; Hu, B.; Lafon, O.; Trebosc, J.; Deng F.; Amoureux, J. P. Double-quantum homonuclear NMR correlation spectroscopy of quadrupolar nuclei subjected to magic-angle spinning and high magnetic field, *J. Magn. Reson.*, **2009**, *200*, 251-260.
39) Zhao, W.; Yi, J.; He, P.; Zhou, H. Solid-State Electrolytes for Lithium-Ion Batteries: Fundamentals, Challenges and Perspectives. *Electrochem. Energy Rev.* **2019**, *2*, 574–605.
40) Provis, J.L. Geopolymers and Other Alkali Activated Materials: Why, How, and What? *Mater. Struct.* **2014**, *47* 11-25.
41) Fletcher, R.A.; MacKenzie, K.J.D.; Nicholson, C.L.; Shimada, S. The Composition Range of Aluminosilicate Geopolymers, *J. Eur. Ceram. Soc.* **2005**, *25*, 1471-1477.
42) Kolousek, D.; Brus, J.; Urbanova, M.; Andertova, J.; Hulinsky V.; Vorel, J. Preparation, Structure and Hydrothermal Stability of Alternative (Sodium Silicate-Free) Geopolymers, *J. Mater. Sci.* **2007**, *42*, 9267-9275.
43) Sekiguchi, K.; Obi, N. Studies on absorption of eutectic mixture. I. A comparison of the behavior of eutectic mixture of sulfathiazole and that of ordinary sulfathiazole in man. *Chem. Pharm. Bull.* **1961**, *9*, 866–872.
44) Liu R. (ed.) Water-insoluble drug formulation. 2nd ed. CRC Press Taylor & Francis Group, USA 2008.
45) Borges, A.F.; Silva, C.; Coelho, J.F.J; Simoes, S. Oral films: Current status and future perspectives II - Intellectual property, technologies and market needs. *J. Control. Release.* **2015**, *206*, 108-121.
46) Nokhodchi, A.; Javadzadeh, Y.; Siahi-Shadbad M. R.; Barzegar-Jalali, M. The effect of type and concentration

of vehicles on the dissolution rate of a poorly soluble drug (indomethacin) from liquisolid compacts. *J Pharm Pharmaceut Sci.*, **2005**, *8*, 18-25.
47) Zauška, Ľ.; Beňová, E.; Urbanová, M.; Brus, J.; Zeleňák, V.; Hornebecq, V.; Almáši, M. Adsorption and Release Properties of Drug Delivery System Naproxen-SBA-15: Effect of Surface Polarity, Sodium/Acid Drug Form and *pH*. *J. Funct. Biomater.* **2022**, *13*, 275.
48) Macku, J.; Kubova, K.; Urbanova, M.; Muselik, J.; Franc, A.; Koutna, G.; Pavelkova, M.; Vetchy, D.; Masek, J.; Maskova, E.; et al. Rational Design of Self-Emulsifying Pellet Formulation of Thymol: Technology Development Guided by Molecular-Level Structure Characterization and Ex Vivo Testing. *Pharmaceutics* **2022**, *14*, 1545.
49) Elena, B.; Pintacuda, G.; Mifsud, N.; Emsley, L. Molecular Structure Determination in Powders by NMR Crystallography from Proton Spin Diffusion, *J. Am. Chem. Soc.* **2006**, *128*, 9555–9560.
50) Salager, E.; Day, G. M.; Stein, R. S.; Pickard, C. J.; Elena, B.; Emsley, L. Powder Crystallography by Combined Crystal Structure Prediction and High-Resolution ^{1}H Solid-State NMR Spectroscopy. *J. Am. Chem. Soc.* **2010**, *132*, 2564-2566.
51) Baias, M.; Widdifield, C. M.; Dumez, J. N.; Thompson, H. P. G.; Cooper, T. G.; Salager, E.; Bassil, S.; Stein, R. S.; Lesage, A.; Day, G. M.; Emsley, L. Powder crystallography of pharmaceutical materials by combined crystal structure prediction and solid-state ^{1}H NMR spectroscopy. *Phys. Chem. Chem. Phys.* **2013**, *15*, 8069-8080.
52) Hruby, M.; Agrawal, K.; Policianova, O.; Brus, J.; Skopal, J.; Svec, P.; Otmar, M.; Dzubak, P.; Stepanek, P.; Hajduch, M. Biodegradable system for drug delivery of hydrolytically labile azanucleoside drugs. *Biomedical Papers-Olomouc* **2016**, *160*, 222-230.
53) Graeser, K.A.; Strachan, C. J.; Patterson, J. E.; Gordon, K. C.; Rades T. Physicochemical Properties and Stability of Two Differently Prepared Amorphous Forms of Simvastatin, *Crystal Growth & Design* **2008,** *8*, 128-135.
54) Greco, K.; Bogner, R. Crystallization of Amorphous Indomethacin during Dissolution: Effect of Processing and Annealing, *Mol. Pharmaceutics* **2010**, *7*,1406–1418.
55) Bell, J.L., Sarin, P.; Provis, J. L.; Haggerty, R. P.; Driemeyer, P. E.; Chupas, P. J.; van Deventer, J. S. J.; Kriven, W. M. Atomic Structure of a Cesium Aluminosilicate Geopolymer: A Pair Distribution Function Study, *Chem Mater* **2008,** *20*, 4768-4776.
56) Hajimohammadi, A.; Provis, J. L.; van Deventer, J. S. J. Effect of Alumina Release Rate on the Mechanism of Geopolymer Gel Formation, *Chem Mater* **2010,** *22*, 5199-5208.
57) Scano P.; Locci E.; Noto A.; Navarra G.; Murgia F.; Lussu M.; Barberini L.; Atzori L.; De Giorgio F.; Rosa MF.; d'Aloja E. ^{1}H NMR metabolite fingerprinting as a new tool for body fluid identification in forensic science. *Magn. Reson. Chem.* **2013**, *51*, 454-462.
58) Kukackova, O.; Dung, NV.; Abbrent, S.; Urbanova, M.; Kotek, J.; Brus, J. A novel insight into the origin of toughness in polypropylene–calcium carbonate microcomposites: Multivariate analysis of ss-NMR spectra, *Polymer* **2017**, *132*, 106-113.
59) Czernek, J.; Brus, J. Polymorphic Forms of Valinomycin Investigated by NMR Crystallography. *Int. J. Mol. Sci.* **2020**, *21*(14), 4907.
60) Müller M, Hansen A, Grimme S. ωB97X-3c: A composite range-separated hybrid DFT method with a molecule-optimized polarized valence double-ζ basis set. *J Chem Phys.* **2023**, *158*, 014103.
61) Paruzzo, F.M.; Hofstetter, A.; Musil, F.; De, S.; Ceriotti, M.; Emsley, L. Chemical shifts in molecular solids by machine learning, *Nat. Commun.* **2018**, *9*, 4501.
62) Cordova, M.; Balodis, M.; Hofstetter, A.; Paruzzo, F.; Nilsson Lill, S.O.; Eriksson, E.S.E.; Berruyer, P.; Simões de Almeida, B.; Quayle, M.J.; Norberg, S.T.; Svensk Ankarberg, A.; Schantz, S.; Emsley, L. Structure determination of an amorphous drug through large-scale NMR predictions, *Nat. Commun.* **2021**,*12*, 2964.
63) Wickramasinghe N. P.; Ishii, Y. Sensitivity enhancement, assignment, and distance measurement in 13C solid-state NMR spectroscopy for paramagnetic systems under fast magic angle spinning, *J. Magn. Reson.* **2006**, *181*, 233–243.
64) Kervern, G.; Steuernagel, S.; Engelke, F.; Pintacuda, G.; Emsley, L. Absence of Curie relaxation in paramagnetic solids yields long 1H coherence lifetimes. *J. Am. Chem. Soc.*, **2007**, *129*, 14118.
65) Pell, A. J.; Pintacuda, G. Broadband solid-state MAS NMR of paramagnetic systems. *Progress in nuclear magnetic resonance spectroscopy*, **2015**, *84*, 33-72.
66) Ji F.; Wang F.; Kobera L.; Abbrent S.; Brus J.; Ning W.; Gao F. The atomic-level structure of bandgap engineered double perovskite alloys Cs2AgIn1-xFexCl6, *Chemical Science.* **2021**, *12,* 1730.
67) Zou, Y., Teng, P., Xu, W., Zheng, G., Lin, W., Yin, J., ... & Gao, F. Manipulating crystallization dynamics through chelating molecules for bright perovskite emitters. *Nature Communications*, **2021**, *12*, 4831.
68) Kuang C., Hu Z., Yuan Z., Wen K., Qing J., Kobera L., Abbrent S., Brus J., Yin C., Wang H., Xu W., Wang J., Bai S., Gao F. Critical role of additive-induced molecular interaction on the operational stability of perovskite light-emitting diodes, *Joule*. **2021**, *5*, 618-630.
69) Chen, H., Zhang, R., Chen, X., Zeng, G., Kobera, L., Abbrent, S., ... & Li, Y. (2021). A guest-assisted molecular-organization approach for >17% efficiency organic solar cells using environmentally friendly solvents. *Nature Energy.* **2021**, *6*, 1045-1053.
70) Zhang, T., Wang, F., Kim, H. B., Choi, I. W., Wang, C., Cho, E., ... & Gao, F. Ion-modulated radical doping of spiro-OMeTAD for more efficient and stable perovskite solar cells. *Science*, **2022**, *377(6605)*, 495-501.
71) Rankin, A. G., Trébosc, J., Pourpoint, F., Amoureux, J. P., Lafon, O. Recent developments in MAS DNP-NMR of materials. *Solid State Nuclear Magnetic Resonance*, **2019**, *101*, 116-143.
72) Hillier, A. D., Blundell, S. J., McKenzie, I., Umegaki, I., Shu, L., Wright, J. A., ... & Watanabe, I. Muon spin spectroscopy. *Nature Reviews Methods Primers*, **2022**, *2*, 4.

Statement about the authorship of the presented research results:

In most of the presented research results (papers D1-D32), the contribution of the author of this thesis (*dr. J. Brus*) was crucial: he designed the methodological concepts, performed the experimental (NMR) measurements, processed, analyzed and interpreted the data, formulated hypotheses and conclusions, wrote the articles predominantly as the first and corresponding author, and supervised the research teams including Ph.D. students (M. Urbanova, L. Kobera, and O. Policianova).

On the other hand, most of the materials and systems studied were synthesized by the coworkers and co-authors of the papers presented. Specifically, polymeric systems the investigation of which is described in the paper D4 were synthesized by the group of *dr. M. Špírková*; in the papers D5, D6 and D11 by the group of *dr. K Kubova*; D7 *dr. A. Strachota*; D8, D9 and D19 *dr. P. Matejicek*; D13 *dr. I. Kelnar*; D15 *dr. W Albrecht*; D16 *dr. M Strečková*; D18 and D20 *dr. K Edström*; D23 *dr. J Dědeček*; and in the paper D29 by the group of *dr. M Hruby*.

Dr. M. Husak has been a key researcher in the development of new methodologies for solving crystal structures from XRPD data (D27 and D28). In this research *Dr. J Brus* contributed substantially to the ss-NMR spectroscopy part, collected and interpreted the NMR data, and wrote and submitted the papers D27 and D28 as the corresponding author.

Other co-authors of the papers included to this dissertation such as *dr. J. Dybal*, *dr. M. Urbanova*, *dr. J. Czernek*, *dr. L. Kobera*, *dr. A. Jegorov*, *dr. I. Sedenkova*, *dr. A. Sturcova*, *dr. D. Hlavata*, *dr. J. Kotek* etc. contributed substantially by performing specific quantum-chemical calculations or by collecting of X-ray, FTIR and other spectroscopic and physicochemical data.

Acknowledgments

I thank to all my colleagues who collaborated with me on the presented research. This work would not have been possible without their valuable help.

Scientometric data	**Jiri Brus**
Researcher ID **G-3459-2014**	**Publications (total): 276** original papers published in impacted journals **(SCOPUS)**
Scopus ID **7003944134**	**First author: 39**
	Corresponding author: 56
ORCID **https://orcid.org/0000-0003-2692-612X**	**Number of citations: 5750** times including self-citations **(SCOPUS)**, **5051** without self-citations **(SCOPUS)**
	***h*-index: 41 (SCOPUS), 38** (without self-citations, **SCOPUS**)